ELECTRICAL PROPERTIES

OF SHEEP PURKINJE STRANDS

Electrical and Chemical Potentials in the Clefts

R. A. Levis, R. T. Mathias, and R. S. Eisenberg
Department of Physiology, Rush Medical College, Chicago, Illinois 60612

ABSTRACT The impedence of sheep Purkinje strands, measured to 3–5 kHz, is interpreted with circuit models based on morphology. The strand is described as a one-dimensional electrical cable. Clefts between myocytes of the strand allow radial current to flow in parallel with current across the outer membrane. A lumped model of the clefts, in which all the cleft membrane is in series with 100 Ω-cm^2, fits only below 20 Hz. Two distributed models, pie and disk, fit at all frequencies with somewhat different (31%) luminal resistivities, but with similar membrane parameters. Series resistance representing the endothelial sheath is small. Simulations of voltage clamp experiments include measured linear parameters and nonlinear membrane channels, as well as radial variation of cleft concentration, membrane flux, voltage, and current. Cleft potential is drastically nonuniform when sodium current flows. Cleft potential is reasonably uniform when calcium and potassium currents flow, but the calcium and potassium concentrations change markedly, enough to turn off the calcium current, even if the calcium channel did not inactivate. We conclude that physiological current flows produce significant nonuniformities in electrochemical potentials in the clefts of this cardiac preparation.

INTRODUCTION

The action potential of sheep Purkinje strands has been extensively studied. The linear electrical properties important in determining the conduction velocity have been measured from the shape of the action potential and the transient response to applied current (Fozzard, 1966; Hellam and Studt, 1974a, b; Schoenberg et al., 1975). The ionic currents underlying the action potential have been studied (reviewed in Noble, 1975; Cranefield, 1975; Fozzard, 1977; and Reuter, 1979) using the voltage clamp method, which, in its traditional form, interprets all the currents as if they arise in a smooth unfolded surface membrane, across which the electrochemical potential is constant and controlled. In this paper we present measurements and simulations that suggest that the electrochemical potential for physiologically important ions cannot be controlled and is not constant during the flow of physiological currents, either during the action potential or during typical voltage clamp experiments.

The structure of Purkinje strands, like the structure of most cardiac tissue, is rather complex (Sommer and Johnson, 1968, 1979; B Eisenberg and Cohen, 1983). A strand consists of many cells electrically coupled one to another by gap junctions, and the cells making up the strand are closely packed, with long narrow extracellular clefts sepa-

rating their membranes. The structural complexities of sheep Purkinje strands are likely to modify ionic current flow during the action potential or voltage clamp: membrane current gains access to the bathing solution only through the clefts, thus making control of concentration and potential unlikely across most membranes (Johnson and Lieberman, 1971; Attwell and Cohen, 1977).

For these reasons, we made inpedance measurements of the electrical properties of clefts and membranes in sheep Purkinje strands. Impedance measurements, interpreted with structurally based theory (Eisenberg and Mathias, 1980), have been used to study the electrical structure of several preparations (e.g., spherical aggregates of cardiac muscle, Mathias et al., 1981a; skeletal muscle fibers, Eisenberg, 1983; epithelia, Clausen et al., 1979; lens of the eye, Mathias et al., 1981b; Rae et al., 1982). Such structural analysis is needed in general to synthesize the properties of an intact preparation, even if the properties and distribution of ionic channels are known from patch clamp measurements (Reuter et al., 1982) or biochemical separation and reconstitution of channels (Coronado and Latorre, 1982).

Impedance results are interpreted in this paper with two topological models of the sheep Purkinje strand, corresponding to different radial distributions of inner membrane along the cleft. The "pie model," introduced by Hellam and Studt (1974a, b) and Schoenberg et al. (1975), was studied further by Schoenberg and Fozzard

(1979). Levin and Fozzard (1981) provide a more rigorous derivation of simple and complex versions of the model. The pie model represents the cross section of a cylindrical Purkinje strand as a sliced pie, each piece of pie being a single cell electrically coupled to its neighbors by gap junctions. The cuts between pieces represent the extracellular space that pervades the tissue. In the pie model, the total volume of the cleft, in a thin annulus of strand of width δr, is independent of radial location; the total cross-sectional area of cleft (available for radial current flow) is also independent of radial location. Thus, the cleft resistance[1] is independent of radial location as well. The pie model implies a radial variation in the morphology of the preparation; the amount of membrane per unit volume depends reciprocally on the distance from the center of the strand.

Our electrical data are also interpreted with a "disk model" of the strand, used previously to describe cardiac muscle by Haas and Brommundt (1980) and skeletal muscle by Falk and Fatt (1964), Adrian et al. (1969), Schneider (1970), Valdiosera et al. (1974), and Mathias et al. (1977). The disk model implies a radially uniform morphology, but the total volume of cleft, in a thin annulus of strand of width δr, varies with radial location. The cross-sectional area of cleft (available for radial current flow) also varies with radial location. Thus, the cleft resistance in the disk model varies radially as well.

Analysis and simulations show that the pie and disk models are difficult, if not impossible, to distinguish experimentally from measurements of voltage such as ours, made in the sarcoplasm, essentially across the surface membrane. Measurements of the average variation of the amount of membrane with radial location would probably distinguish between the pie and disk models of the average strand. Measurements of the radial variation of voltage across the cleft membrane would also probably distinguish between the models.

Our impedance measurements showed that the two membrane systems of the strands, the surface and the cleft membranes, contributed quite differently to the overall properties of the preparation. The surface membranes typically comprised only 10% of the membranes of a strand, and they were in series with a small resistance of ~ 5 Ω-cm^2. The other membranes, some 90%, lined the clefts and were in series with the substantial resistance from the small volume of the solution filling the clefts. The resistance in series with any particular channel in the cleft membrane depended on the radial location of the channel, because the distance current had to flow in the clefts

depended on how far the channel was from the edge of the strand: the cleft membrane is distributed along the resistance of the cleft. The resistivity of the solution in the clefts was found to be close to that of the extracellular bathing solution, between 41 Ω-cm and 59 Ω-cm, depending on the model used to represent the strand. When small, slow currents flow across the cleft membrane, one might wish to represent the cleft crudely as a single lumped resistance, some 100 Ω-cm^2, referred to the area of unfolded outer membrane for a strand of ~ 100 μm diam.

Simulations of voltage clamp, using measured parameters of sheep Purkinje strands, confirm earlier calculations (Schoenberg and Fozzard, 1979; Haas and Brommundt, 1980): the distributed series resistance presents severe problems for voltage clamp measurements of sodium currents, whether the sodium current is attenuated by experimental interventions or not. In fact, the potential within the clefts is essentially uncontrolled in both situations. Simulations of the secondary inward current suggested that substantial control of transmembrane potential is possible when current flows through this predominantly calcium channel.

Simulations and analysis of the electrodiffusion of calcium and potassium ions in the clefts and sarcoplasm of the strand were also performed. The analysis yielded a simple approximation to the initial rate of change of cleft concentration. The simulations allowed a radial distribution of cleft concentration, cleft potential, current flow, and membrane fluxes. As expected from the approximate expression and lumped simulations of concentration changes (e.g., Adrian and Freygang, 1962a; Attwell et al., 1979; Almers et al., 1981), significant changes in potassium and calcium concentration occurred during physiological activity, whether clamped or natural. Calcium concentration showed dramatic depletion in the cleft with an initial rate of 33 mM/s; accumulation sometimes also occurred in the sarcoplasm, depending on the intracellular buffering of calcium concentration. The changes in concentration were large compared with initial concentrations and had substantial effects on the interpretation of currents recorded in the voltage clamp. For example, the depletion of calcium was enough to explain the turn-off of calcium current without invoking the inactivation process that Reuter et al. (1982) reported in single channels. Similar changes in concentration must occur during the action potential in the sheep Purkinje strand and significantly affect its properties. Levis (1981) includes more details of the impedance measurements and the models used to interpret them.

THEORY

The Longitudinal Spread of Potential

We define $x = 0$ at the location of the microelectrode that injects current I. The ends of the strand are at $x = l_1$ and $x = -l_2$. The length of the strand was $l_1 + l_2$. The potential $V(x)$ at any longitudinal location x

---

[1]This cleft resistance is given by $\delta(r)R_e/[(\tau(V_c/V_F)S_r(r)]$, in ohms. Eq. A2 and Table A1 of the Appendix shows that $S_r(r)$ is radially independent in the pie model, but radially dependent in the disk model, see Appendix.

within the sarcoplasm was approximated by the differential equation (Jack et al., 1975) for one-dimensional current flow in a transmission line

$$\frac{d^2 V}{dx^2} - \gamma^2 V = -r_i I \delta(x); \qquad \gamma \equiv \sqrt{r_i y \xi_s^2} \qquad (1)$$

where r_i is the longitudinal resistance of a unit length of strand (Ω/cm), produced by a combination of the resistance of the cytoplasm and the resistance of the gap junctions joining Purkinje cells. These equations treat the longitudinal impedance as purely resistive (Levis, 1981, pp. 47–66).[2] $\delta(x)$ is the Dirac delta function and $\gamma(j\omega)$ is the longitudinal propagation constant, which is the frequency domain generalization of the dc length constant $\lambda = 1/\gamma(0)$. The shunt admittance $y\xi_s^2$ (S/cm) in a unit length of strand describes all the pathways by which current can flow from the cytoplasm to the extracellular bathing solution (see Fig. 1, which includes the surface membrane for completeness). ξ_s is the folding factor of the surface membrane; ξ_s^2 appears in Eq. 1 because the folding factor is assumed to be the same in the longitudinal and circumferential directions. The shunt admittance y describes the total current flowing out of the strand. The current flows through the surface or cleft membranes and then through the series resistance r_s (Ω-cm) external to, and in series with, the myocytes of the strand:

$$y = \frac{y_m + y_c}{1 + r_s(y_m + y_c)}. \qquad (2)$$

The accuracy of this simplified treatment of radial and longitudinal current flow (introduced by Falk and Fatt, 1964) has been evaluated by Eisenberg and Johnson (1970), Eisenberg et al. (1979), and Peskoff (1979). The admittance (S/cm) of the surface membrane in a unit length of strand is $y_m \xi_s^2$ where $y_m = g_m + j\omega c_m$, and g_m (S/cm) and c_m (F/cm) are the corresponding conductance and capacitance. The angular frequency in (radians per second) $\omega = 2\pi f$, where f is the frequency in Hz; $j = \sqrt{-1}$. The admittance $y_c \xi_s^2$ is the ratio of the total current flowing out of the clefts (in a unit length of strand) to the voltage $V(x)$ in the cytoplasm. This term represents the entire contribution of the clefts and inner membranes to the electrical properties of the strand. The precise description of the admittance of the clefts depends on the model adopted for their structure, as we discuss below. Each model will produce a different functional form, indicated by different subscripts, for y_c. Each function must be substituted into Eq. 2 and 4 to allow comparisons of the model with experimental data.

The specification of the longitudinal spread of potential is completed by the boundary conditions

$$\left.\frac{dV}{dx}\right|_{x=l_1} = 0 = \left.\frac{dV}{dx}\right|_{x=-l_2}. \qquad (3)$$

These boundary conditions, which state that no longitudinal current flows at the end of the strand, have been widely used to describe the end of a skeletal muscle fiber (Adrian and Freygang, 1962a) particularly when using the three microelectrode voltage clamp (Adrian and Freygang, 1962b; Adrian et al., 1970; Changler et al., 1976). Milton et al. (1982) have recently called attention to this assumption by showing that a large amount of longitudinal current flows at the end of a frog sartorius fiber,

[2]Freygang and Trautwein (1970) concluded that the longitudinal imped-ance included a significant reactance. Levis showed this conclusion to be unwarranted: (a) the measurements with microelectrodes assumed the electrodes had zero longitudinal separation; (b) the measurements with the oil gap, even if taken at face value, imply a longitudinal phase shift with a maximum value of only a few degrees at 2–5 kHz, too small to be resolved by our techniques and of dubious physiological significance.
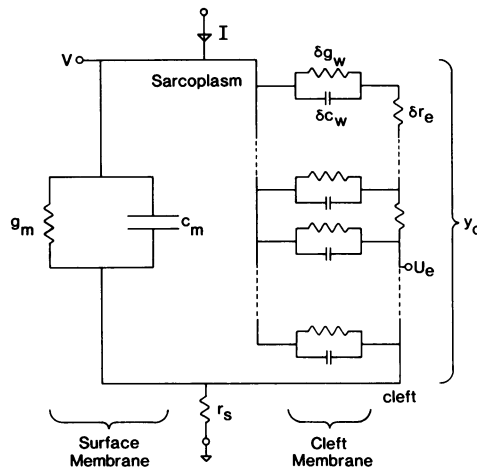

FIGURE 1   A circuit diagram of the admittance of a $1/\xi_s$ length of strand. The current I is injected by a microelectrode. The voltage recorded by the microelectrode is $V(x)$. Current leaving the cytoplasm can flow out of the strand in two ways. It can flow through the cleft membrane, and then through the resistance of the cleft, together represented by the admittance y_c. Or it can flow across the surface membrane, represented by the admittance y_m. Current through both pathways reaches the bath elec-trode after flowing through the resistance r_s of the bathing solution.

because of the large amount of membrane involved in the myotendon junction (Milton and Eisenberg, personal communication). We assume that longitudinal currents at the end of our Purkinje strand are small, since we hope our strands are well healed, with gap junctions, desmosomes and so on not permitting substantial current flow.

The solution of these equations is

$$Z(x, j\omega) \equiv \frac{V(x, j\omega)}{I(j\omega)} =$$

$$\left(\frac{r_i}{\gamma}\right) \frac{\cosh(\gamma x) - \tanh(\gamma l_1)\sinh(\gamma x)}{\tanh(\gamma l_1) - \tanh(\gamma l_2)}. \qquad (4)$$

Lumped Model

The first cleft model considered is the lumped model (Falk and Fatt, 1964; Fozzard, 1966; Freygang and Trautwein, 1970; Valdiosera et al., 1974). This model is justified more by its mathematical simplicity than its anatomical plausibility. There is no morphological basis for a lumped resistance at the perimeter of the strand, dominating access to the clefts. Rather, the lumped model is important because it is the limiting form of more plausible models, useful when the radial potential gradient along the clefts is small (see discussion and references in Mathias et al., 1977). The admittance of the lumped model is

$$y_{cL} = \frac{1}{r_{cL} + \dfrac{1}{\pi a^2 \overline{Y}_w}} \qquad (5)$$

where $\overline{Y}_w = (S_c/V_F)(G_w + j\omega C_w)$.

S_c/V_F (cm^2/cm^3) is the total surface of clefts in the strand divided by the total volume of the strand; G_w (S/cm^2) and C_w (F/cm^2) are the specific conductance and capacitance of the membrane of the cleft; $\overline{Y}_w$ (S/cm^3) is the admittance in a unit volume of strand; r_{cL} (Ω-cm) is the resistance in series with just the cleft membranes, in a unit length of strand. a (cm) is the radius of the strand.

Disk Model

The admittance of the disk model is given by

$$y_{cd} = 2\pi a \frac{\Gamma_d}{r_{cd}} \frac{I_1(\Gamma_d a)}{I_0(\Gamma_d a)} \tag{6}$$

where I_0 and I_1 are modified Bessel functions of orders zero and one (Abramowitz and Stegun, 1964); the radial propagation constant for the disk model Γ_d is the frequency domain generalization of the radial length constant; and r_{cd} is an effective radial resistivity:

$$\Gamma_d = [r_{cd}\overline{Y}_w]^{1/2} \qquad r_{cd} = \frac{R_e}{\tau_d(V_c/V_F)}. \tag{7}$$

R_e (Ω-cm) is the actual resistivity of the solution in the clefts; (V_c/V_F) is the total volume of clefts in a strand divided by the total volume of strand.

The effective radial resistivity depends on the resistivity of the solution within the clefts, the volume fraction of the clefts, and the tortuosity factor τ_d, as described in Eq. 7. Mathias (1983) determines the tortuosity of a number of biologically interesting geometries, including the geometry of anisotropic clefts branching between elongated cells (Mathias, 1983, Eq. 14). The tortuosity factor in that case depends on the size of the unit cell in the radial and circumferential directions (Δx and Δz, respectively for the rectangular coordinate system illustrated in Mathias, 1983) and the amount of wiggling of the clefts in the radial and circumferential directions ξ_r and ξ_z, respectively. The wiggle factor, called the folding factor in Hellam and Studt (1974a, b) and Mobley and Page (1972) is the ratio of the actual path length for current flow in a given direction in the unit cell to the dimension of the unit cell in that direction. The appropriate expression for the tortuosity factor for the disk model of a Purkinje strand is then

$$\tau_d = \frac{1}{2\xi^2} \qquad \text{for } \xi_r = \xi_z = \xi. \tag{8}$$

The right-hand expression is appropriate if, but only if, the branching and wiggling of the clefts are isotropic, that is, if they are the same in the circumferential and radial directions. Purkinje strands and isotropic within the accuracy of available morphological measurements (Hellam and Studt, 1974a), mostly from unstretched strands.

The Pie Model

We write the admittance of the pie model in terms of morphometric parameters S_c/V_F and V_c/V_F to facilitate comparison of the pie and disk models for one particular Purkinje strand.

For the pie model, the surface-to-volume ratio and volume fraction of clefts in the entire strand is

$$\frac{S_c}{V_F} = \frac{2n\xi_r\xi_z}{\pi a}; \qquad \frac{V_c}{V_F} = \frac{n\xi_r\xi_z w}{\pi a} \tag{9}$$

where n is the average number of clefts (not necessarily an integer) and w is the average width of a cleft. Levis (1981, pp. 67–72) shows that this formulation of the pie model is identical to that of Levin and Fozzard (1981). These equations define the morphometric parameters for the clefts in an entire strand, assuming that the membrane wiggling in the clefts has a "wavelength" much longer than the width of the cleft (see Fig. C14 of Levis, 1981). Thus, stereological procedures used to estimate these parameters must uniformly sample the entire strand.

The admittance of the pie model is called y_{cp} here and is given by

$$y_{cp} = 2\pi a \frac{\Gamma_p}{2r_{cp}} \tanh(\Gamma_p a) \tag{10}$$

where, with the assumption of isotropic wiggling,

$$\Gamma_p = (r_{cp}\overline{Y}_w)^{1/2}; \qquad r_{cp} = \frac{R_e}{\tau_p(V_c/V_F)}; \qquad \tau_p = \frac{1}{\xi^2}. \tag{11}$$

Mathias (1983, Eq. 15) derives the expression for the tortuosity factor in unbranched clefts in a slab structure. The Appendix to this paper extends that derivation to the closely related pie model, in which unbranched clefts are packed into a circular cylinder, and all clefts allow radial current flow. In the disk model the clefts are branched, with half of the clefts not allowing radial current flow. Thus, the tortuosity factor of the disk model is expected to be exactly half that for the pie model, as is shown in Eqs. 8 and 11. In the more complex models of Schoenberg and Fozzard (1979) and Levin and Fozzard (1981), some clefts carry no radial current; thus, the tortuosity factor for these models is expected to be between that of the pie and disk model.

METHODS

Preparation

Sheep hearts were obtained from a local slaughterhouse with the help of Dr. H. Fozzard and his associates, whose assistance we acknowledge with pleasure. The heart was frequently still beating when removed immediately (usually within 2 min) after the sheep was slaughtered. While still at the slaughter house, the atria were removed and the ventricles partially cut open and rinsed with cold Tyrode solution consisting of either 137 mM NaCl, 5.4 mM KCl, 2 mM $CaCl_2$, 1 mM $MgCl_2$, 13.4 mM $NaHCO_3$, and ~2 mM NaH_2PO_4 or 150 mM NaCl, 5.4 mM KCl, 2.7 mM $CaCl_2$, 1 mM $MgCl_2$, 11 mM glucose, 3 mM NaOH, and ~5 mM HEPES (pH 7.4). Upon return to the laboratory (after ~1 h), Purkinje strands were dissected free from the ventricular mass with as little stretching as possible. Whenever available, slender (100–200 μm diam) unbranched strands, longer than 1 cm, were chosen for impedance measurements. We expected that thicker or branched strands could not be described by the topological models considered here (Sommer and Johnson, 1968; Valdiosera and Mendiola, 1981).

Strands were mounted unstretched underneath a network of nylon threads running perpendicularly to the long axis of the strand and spaced 1.5–2 mm apart. The threads were sufficiently taut to prevent the Purkinje strands from moving; usually they were not taut enough to damage the tissue. 95% O_2, 5% CO_2 was bubbled through the Tyrode solution containing phosphate buffer; pure O_2 was bubbled through the solution containing HEPES buffer. The flow of gas was interrupted when impedance measurements were made to avoid ripples and resulting electrical artifact. Temperature was maintained between 33° and 37°C.

Current was applied, and voltage recorded, with micropipettes filled with 3 M KCl that had resistances of 10–20 MΩ. The voltage-measuring amplifier was a feedback follower, as described in Mathias et al. (1979, 1981) and Levis (1981). In almost all experiments, the voltage electrode was shielded with silver paint to within 50–200 μm of the tip, and the paint in turn was insulated with varnish to prevent electrical contact between the grounded paint and the bath. The natural frequency of the voltage-recording circuit was between 10 and 30 kHz, depending on the amount of unshielded electrode and the resistance of the microelectrode. The usable bandwidth of the voltage-recording amplifier can be substantially extended by the calibration procedure of Mathias et al., 1979.

The feedback follower circuit functioned by driving the bath to the negative of the potential at the tip of the electrode, thus keeping the electrode tip at virtual ground. The appropriate output signal was then the bath potential, measured close to the site of impalement by the voltage microelectrode. This signal was measured by a "differential electrode," a microelectrode of 30–50 μm tip diam filled with the bathing solution and connected to a voltage-follower (unity gain) circuit. The bandwidth of the differential electrode plus recording circuit was extended by shielding the electrode with silver paint connected to the output of the follower. In some

TABLE I
CIRCUIT PARAMETERS OF THE DISK MODEL

Strand	Resting potential	Radius	$G_w - G_m$	C_m	C_w	R_s	r_e	R_e
	mV	μm	$\mu S/cm^2$	$\mu F/cm^2$	$\mu F/cm^2$	$\Omega\text{-}cm^2$	$\Omega\text{-}cm$	$\Omega\text{-}cm$
1	−78	73	59	(0.87)*	0.87	2‡	65	56
2	−83	55	37	1.2	0.60	--	59	49
3	−69	45	43	1.0	0.94	6	80	67
4	−77	68	63	(1.7)	1.7	3	46	38
5	−77	53	63	1.4	0.66	--	34	28
6	−76	52	100	(0.59)	0.59	15	108	87
7	−74	50	59	(0.82)	0.82	2	83	69
8	−78	55	67	(1.47)	1.5	4	96	82
9	−75	48	29	0.98	0.54	--	232	192
10	−84	60	53	(0.88)	0.88	6	77	64
11	−80	63	48	(0.81)	0.81	3	63	51
12	−73	54	110	(0.70)	0.70	5	43	36
13	−81	61	77	(1.2)	1.2	6	34	28
14	−85	56	91	1.5	0.72	--	37	28
15	−66	64	37	(0.70)	0.70	10	28	23
16	−64	73	36	(1.48)	1.5	9	63	51
17	−77	54	100	(0.91)	0.91	8	51	41
Mean	−76	58	63	1.1	0.89	6	71	59
SEM	1	2	6	0.1	0.08	1	12	10

*Parentheses indicate that the value of C_m was set equal to the value of C_w, as described in the text.

‡Dashes (--) indicate that R_s was set equal to zero, as described in the text. These values were excluded from the mean.

TABLE II
CIRCUIT PARAMETERS OF THE PIE MODEL

Strand	Electrode separation	R_i	$G_w - G_m$	C_m	C_w	R_s	r_e	R_e
	μm	$\Omega\text{-}cm$	$\mu S/cm^2$	$\mu F/cm^2$	$\mu F/cm^2$	$\Omega\text{-}cm^2$	$\Omega\text{-}cm$	$\Omega\text{-}cm$
1	280	(120)*	67	(0.86)‡	0.86	2§	23	38
2	180	105	36	1.8	0.57	--	20	33
3	210	(120)	43	1.2	0.89	--	28	46
4	340	(120)	63	(1.6)	1.6	2	16	26
5	230	92	63	1.6	0.61	--	12	21
6	210	(120)	83	(0.60)	0.60	9	36	59
7	100	(120)	56	1.3	0.68	--	30	49
8	320	92	67	(1.4)	1.4	1	28	46
9	200	63	28	1.2	0.53	--	95	156
10	220	(120)	50	1.2	0.78	--	31	51
11	150	114	48	(0.80)	0.80	4	20	33
12	300	(120)	110	(0.68)	0.68	2	15	26
13	250	(120)	77	(1.1)	1.1	5	12	21
14	230	77	91	1.8	0.72	--	16	26
15	250	(120)	37	(0.73)	0.73	7	11	18
16	200	208	34	(1.44)	1.4	5	22	36
17	180	(120)	91	(0.88)	0.88	4	19	31
Mean	226	110	61	1.2	0.88	4	26	41
SEM	15	7	6	0.1	0.08	1	5	8

*Parentheses indicate that the value of R_i was set equal to 120 Ω-cm, see text.

‡Parentheses indicate that the value of C_m was set equal to the value of C_w, as described in the text.

§Dashes (--) indicate that R_s was set equal to zero, as described in the text. These values were excluded from the mean.

experiments (strands 2, 5, 7, 14 in Tables I and II), measurements were made both with the voltage microelectrode inside the myocytes of the Purkinje strand and with the microelectrode between the outermost myocytes and the connective tissue sheath that forms the outer annulus of the strand. To completely remove the series resistance of the sheath and bath, the impedance measured in the latter situation was subtracted from the intracellular impedance, after correction for the change in the resistance of the voltage electrode, which often accompanies removal from the cell. With these precautions the measurements seem reliable (i.e., have negligible phase error) to 3–5 kHz. Parameter estimates from curve fits to these data did not differ from mean values.

Following the procedures to avoid capacitive shunting to applied current (Falk and Fatt, 1964; Valdiosera et al., 1974), we measured impedance at high frequencies by comparing the voltage at the top of the current microelectrode with the voltage recorded from the cell interior. This procedure gives a scaled version of the impedance; thus, it gives the correct phase angle, but a multiple of the magnitude of the impedance. The multiplier is determined by measuring impedance directly at low frequencies, using direct measurements of applied current (Mathias et al., 1979) and voltage. The multiplier is simply the resistance of the current electrode, which has been shown to be frequency independent by Valdiosera et al. (1974).

Impedance was measured and fit with theory as described by Mathias et al. (1979, and 1981). Smoothing of the data was not necessary because of the relatively low variance of the raw data; wild-point editing at multiples of 60 Hz was usually required, however.

Estimates were needed of (a) strand length (b) strand diameter, (c) electrode separation, and (d) electrode position with respect to the ends of the strand. These measurements were always somewhat uncertain.

The physical length of the strand was easy to measure, but this does not necessarily correspond to the electrical length, and so is not reported. As much as 1 mm at each end of the strand might be dead, or electrically uncoupled from the cells in the center of the strand. In most experiments, an effort was made to measure the electrical length by repeated impalement. This was never less than 6 mm and in all but two cases was >1 cm. However, such experiments were not always conclusive, because of the difficulty in penetrating the sheath surrounding the muscle cells. In some cases, it seemed as if the nylon threads used to hold the strand were sufficiently taut to damage individual myocytes and thus disrupt electrical continuity along the strand.

The diameter of the strand was estimated using transmitted light and a dissecting microscope, which allowed the inner muscle mass to be clearly distinguished from the surrounding connective tissue in reasonably slender strands. Such measurements are less than ideal because the projected image of the muscle mass must be assumed to be essentially circular in cross section. The strand may also be nonuniform or branch along its length, leading to either over- or underestimates in membrane area if two bundles cohabited in one connective tissue sheath, depending on the details of their electrical connection. For this reason, strands where the estimate of the specific capacitance of the cleft membranes was too small ($C_w < 0.4 \mu F/cm^2$) or too large ($C_w > 3.0 \mu F/cm^2$) were rejected.

The typical electrode separation of 150–200 μm was chosen to minimize three-dimensional effects (Eisenberg and Johnson, 1970) without producing too much longitudinal decrement. The distance between the locations where the electrodes penetrated the connective tissue sheath could be measured with negligible error. But the true separation was only estimated, because the tips of the electrodes could not be clearly visualized through the sheath.

Because of the various errors involved in estimating electrode location, strand length, diameter, and electrode separation, we were not surprised that some of our data sets could not be fit with the measured values and reasonable circuit parameters. Almost all of the data sets could be fit with reasonable circuit parameters if we used arbitrary but reasonable values of the strand length, diameter, and/or electrode separations in the curve fitting procedure. Data sets fit with arbitrary parameters are not presented in this paper.

Simulations

Numerical computations including voltage-dependent ionic conductances were performed on a Nova 3 minicomputer (Data General Corp., Southboro, MA) with hardware floating-point unit. The potential across the cleft membrane U was computed by dividing the clefts radially into 50 shells of equal thickness δr, with the transmembrane potential computed at a node in the center of each shell. In a standard strand of 60-μm radius, the radial locations of the nodes were 0.6, 1.8, 3.0, . . . , 58.2, and 59.4 μm. This shell construction corresponds to an equivalent radial cable with the amount of cleft membrane and radial resistance in each shell computed from the disk or pie models at the location of the node. The radial resistance between nodes is the sum of the half resistances corresponding to each nodal location. For example, the luminal resistance between shells (i.e., nodes) k and $k + 1$ in the disk model is

$$\left(\frac{1}{2\pi(k - 1/2)\delta r} + \frac{1}{2\pi(k + 1/2)\delta r} \right) \frac{\delta r}{2} r_{ed}. \qquad (12)$$

At the center of the strand, the boundary condition is $(\partial U/\partial r)_{r=0} = 0$. At the surface of the strand the boundary condition for the radial cable is given by Eq. A3 with $U_c(a, x; t) = 0$, $V(x; t) = $ a constant, independent of time and longitudinal location. In other words, the surface membrane was assumed to be clamped to a known and time-independent voltage. The currents across the surface membrane were assumed to arise from a membrane with area of 1.8 cm^2 for each 1 cm^2 of unfolded membrane.

The shell construction leads to a system of 50 simultaneous equations (see Carnahan et al., 1969; Joyner et al., 1978, and references cited there). We approximate the second derivative (with respect to r) by a second-order central difference and the first derivative (with respect to time) by a first-order forward difference. Then, the potentials in each shell at time $t + \delta t$, namely $U(k\delta r; t + \delta t)$, are determined by the potentials in the neighboring shells at the previous time $U([k - 1]\delta r; t)$, $U(k\delta r; t)$, $U([k + 1]\delta r; t)$, and the various nonlinear conductances and other circuit parameters associated with these voltages at time t. (The ionic conductances are described precisely later in this paper.) Iteration starts with the initial conditions that give the voltage at all radial locations at time zero. For computations of the sodium conductance $\delta t = 10 \mu$s; for computations of the secondary inward, i.e., calcium conductance, $\delta t = 40 \mu$s.

Integration of the field equations for electrodiffusion follows the same plan using central differences to approximate the radial second derivative of the calcium or potassium concentration.

Simulations of Electrodiffusion

Simulations of the electrodiffusion of calcium and potassium ions were performed. The flux of sodium was not expected to last long enough to have substantial effects. The maximum depletion of sodium would be some 3–5 mM (out of 140 mM resting concentration) in a typical cardiac action potential, if significant sodium flux occurred only during the fast inward current.

We describe electrodiffusion with a distributed model, of both cleft potential and cleft concentration (Lammel, 1981), analogous to the distributed models that describe strictly electrical properties of syncytial tissues. The model describes solute movement in the extracellular and intracellular space by a combination of conservation laws and the Nernst-Planck equations. It also involves a model of the Hodgkin-Huxley type to describe the potassium or calcium channel and the resulting solute flux across the membrane.

The concentration of ions in the clefts is described by the Nernst-Planck equation (see Sten-Knudsen, 1978), written here for calcium:

$$J_{Ca}(r) = -d_{Ca}\left(\frac{\partial Ca_e}{\partial r} + \frac{2F}{RT} Ca_e \frac{\partial U_e}{\partial r} \right) \qquad (13)$$

where R is the gas constant; T is the absolute temperature; and F is Faraday's constant. U_e is the potential in the extracellular space; $J_{Ca}(r)$ is the flux of calcium in the extracellular space (in moles times square centimeters per second); Ca_e is the concentration of calcium in the extracellular space (in moles per liter); d_{Ca} is the effective diffusion coefficient for calcium in the clefts determined from measurements of the effective resistance of the clefts.

We estimate the effective diffusion coefficient d_{Ca} from the effective diffusion constant for NaCl, which is in turn estimated from the measured effective resistance r_e of the clefts in either the disk or the pie models:

$$d_{Ca} = \frac{D_{Ca}}{D_{NaCl}} d_{NaCl} = 0.53 d_{NaCl}; \quad d_{NaCl} = \frac{RT}{F^2} \frac{10^3}{C_e} \frac{1}{r_e}. \quad (14)$$

In these equations, C_e is the osmolarity of the solution of the extracellular space, close to the osmolarity of the extracellular NaCl in our case; D_{Ca} and D_{NaCl} are the diffusion coefficients for calcium and NaCl at the concentration found in our Ringer's solution tabulated in Parsons (1959, pp. 79–80), and the factor of 10^3 reconciles chemical units of moles per liter and our spatial units of centimeters. The conservation equation in the extracellular space is

$$\frac{V_c}{V_F} \frac{\partial Ca_e}{\partial t} = \nabla J_{Ca} + \frac{10^3}{2F} \frac{S_c}{V_F} g_{si}(U - E_{si})$$

$$+ \text{convection terms.} \quad (15)$$

In these equations, ∇ is the divergence operator; the morphometric parameters have their usual significance; U is the potential across the cleft membrane, $U = V - U_e$, see Eq. A3; g_{si} and $E_{si} = (RT/2F) \ln (Ca_e/Ca_i)$ are, respectively, the conductance and the equilibrium potential of the slow inward current. Convection is neglected because the changes in osmolarity are small for calcium currents. For potassium currents, convection effects may not be negligible and a more precise analysis would explicitly include water flow, net ionic flux, and charge balance. Eq. 13 and 15 can be combined to give a single field equation describing calcium concentration in the clefts of syncytia. The field equation is made complete by a description of calcium concentration in the cytoplasmic medium and the distribution of electrical potential (see Eq. A1 and A2) in both cytoplasm and clefts.

A simplified version of Eq. 15 is useful and, in fact, provided much of our motivation for the analysis of electrodiffusion. The initial rate of concentration change in the clefts can be calculated by neglecting extracellular diffusion, because the extracellular concentration gradient is small at short times. Then, we have

$$\left. \frac{dCa_e(t)}{dt} \right|_{t=0} \simeq 10^3 \frac{V_F}{V_c} \frac{S_c}{V_F} \frac{g_{si}}{2F} (U - E_{si}). \quad (16)$$

Typical values might be $g_{si} \simeq 10^{-4}$ S/cm^2; $w \simeq 3 \times 10^{-6}$ cm; and $U - E_{si} \simeq 100$ mV, giving an initial rate of depletion of calcium of $\sim$33 mM/s.

Equivalent field equations have been derived to describe the calcium concentration in the intracellular space, but they can be substantially simplified here because radial diffusion is insignificant inside the myocytes, as shown by a perturbation expansion of the field equations for electrodiffusion (Mathias, unpublished information) equivalent to that used to solve syncytial electrical problems. The resulting equation describing concentration changes in the intracellular medium is

$$\left(1 - \frac{V_c}{V_F}\right) \frac{\partial Ca_i}{\partial t} = - \frac{10^3}{2F} \frac{S_c}{V_F} g_{si}(U - E_{si}). \quad (17)$$

The factor $1 - (V_c/V_F)$ is not significantly different from unity in sheep Purkinje strands, although it may well be in other preparations. In applications to those preparations, the reader should be aware that we

have not systematically included such factors in our definition of sarcoplasmic parameters, e.g., intracellular resistivity.

The computations of electrodiffusion presented here are with the disk model; we expect that computations with the pie model would give similar results.

RESULTS

Fig. 2 shows the phase angle and magnitude of the impedance recorded from a typical strand. The lumped model produced a poor fit to this and all other data sets. The lumped model could approximate the phase data only at the low and intermediate frequencies (say 0–20 Hz) where the disk, pie, and lumped models are indistinguishable. It is not surprising that the lumped model provides an inadequate description of a sheep Purkinje strand: there is no structure in the clefts likely to produce a dominating access resistance.

In contrast to the phase data, the magnitude data were reasonably described by the lumped model over the entire frequency range, as one might expect given the known insensitivity of magnitude plots to the details of models containing only resistors and capacitors (e.g., Eisenberg, 1983, Figs. 1 and 2).

Fits with Distributed Models of the Clefts

Pie and Disk Models. Typical fits of the pie and disk model are shown in Fig. 3. The difference in fit of the models depends on details of the curve fitting procedure and so is not considered significant. Tables I and II present
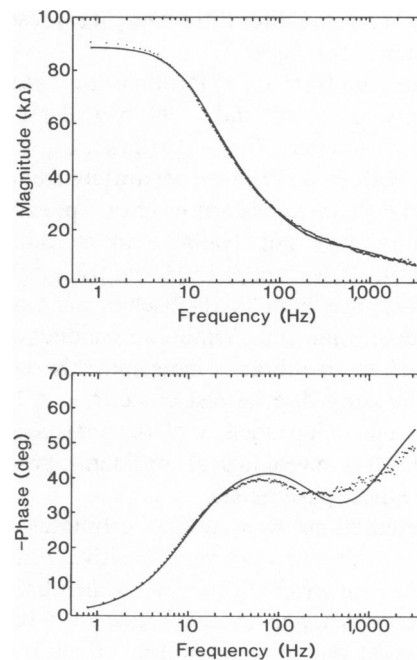

FIGURE 2 The phase angle and magnitude of the admittance of a typical strand, showing the fit of the lumped model. Note the serious misfit of the data.
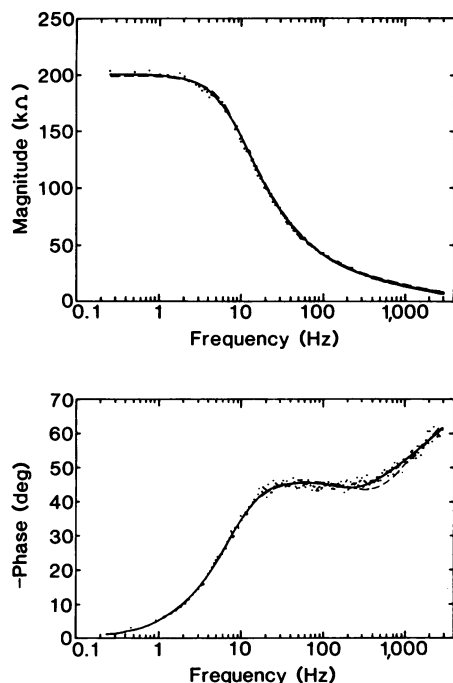
FIGURE 3 The phase angle and magnitude of the admittance of a typical strand, showing the fit of the disk (———) and pie (----) models. Note that both fits are quite satisfactory and essentially indistinguishable except in the values of the parameters producing the best fit (see Tables I and II). The microelectrodes were 2.5 mm from the end of a 1-cm long strand.

the data from 17 strands, showing the specific electrical parameters and effective radial resistivity measured in each case. The morphometric data used in these curve fits were taken from the literature and are presented and discussed later in this paper.

Impedance data from sheep Purkinje strands at a resting potential between −70 and −90 mV determine four independent parameters, $G_m = g_m/(2\pi a)$, $C_m = c_m/(2\pi a)$, R_e, and C_w, with R_i determined separately from measurement of the DC length constant whenever possible. (When sufficient data were not available to measure the DC length constant, R_i was set to 120 Ω-cm [Schoenberg et al., 1975.]) Impedance data in themselves are not sensitive enough to determine the membrane conductance of the cleft and surface membranes independently, nor do they determine the lumped series resistance $R_s = r_s \, 2\pi a$ outside the preparation[3] independently of the surface membrane capacitance. Thus, physiological considerations are needed to determine these parameters.

Model calculations showed that estimates of surface membrane capacitance were very sensitive to the value of the resistance r_s in series with the outer membrane. Values of the series resistance in the range of 0.05% of the membrane resistance have substantial effects on the phase

[3]This lumped resistance R_s presumably arises in the connective tissue sheath and bathing solution outside the strand and should not be confused with the resistance or resistivity of the clefts.

plot at frequencies above 300 Hz (Levis, 1981, Fig. C18) because the membrane admittance increases rapidly with frequency. Indeed, if the series resistance were 0.1% of the membrane resistance we report, it would have about a 50% effect on the admittance and produce a 45° phase shift at a frequency of 10 kHz! For this reason, the series resistance r_s was included in all our theoretical models (see Eq. 2), and we tried to estimate its value by our usual curve fitting procedures. Estimates of the series resistance of strands 2, 5, 7, and 14 were not included in the mean or analysis of sheath resistance, because of the subtraction procedure used, as described in Methods.

Measurements of impedance to 10–20 kHz would be needed to determine C_m, C_w, and R_s independently, but our measurements of the impedance of Purkinje strands were not considered reliable at frequencies above 3–5 kHz. We therefore adopted the following procedure to determine as many parameters as possible with the data available. The specific capacitance of the surface membrane C_m was set equal to the specific capacitance of the walls of the clefts C_w, and the values of C_m (now equal to C_w) and R_s were determined by curve fitting. This procedure produced reasonable values of parameters in some two-thirds of the strands. In the other one-third, the resulting estimate of the series resistance was negligible or negative. In those cases (indicated in the Tables) the value of R_s was set to zero; it was then possible to estimate C_m and C_w independently. The data in Tables I and II seem to indicate different values for C_m and C_w, which in turn might reflect errors in our morphometric assumptions. Unfortunately, the significance of these estimates is substantially reduced by the unknown cause of variation in R_s.

Consider next estimation of the specific conductance of the cleft and surface membranes. The surface and cleft membranes of Purkinje myocytes are distinguished morphologically by the extracellular space they abut (although they may well contain different amounts of junctional specializations); thus, we expect the specific membrane conductances of the two membranes to be similar, as was assumed by Levin and Fozzard (1981). Some such assumption is necessary as well as reasonable. Because of the large value (compared with the radius) of the DC length constant of the clefts $1/\Gamma(0)$, the surface and cleft membranes are essentially in parallel in the sheep Purkinje strand at DC. In that case, the specific membrane conductances of the cleft and surface membranes G_w and G_m have essentially the same effect on the phase plots, so they cannot be estimated independently. We have not actually set G_w and G_m equal; rather we set $G_w = G_m(C_w/C_m)$ to take into account variance in cleft membrane area from strand to strand. We suspect that the substantial variance in our estimations of C_w and G_w reflects the variance in cleft membrane area more than the variance in specific electrical parameters. Our data are fit with one set of morphometric parameters, while the area of cleft membrane varies from strand to strand.
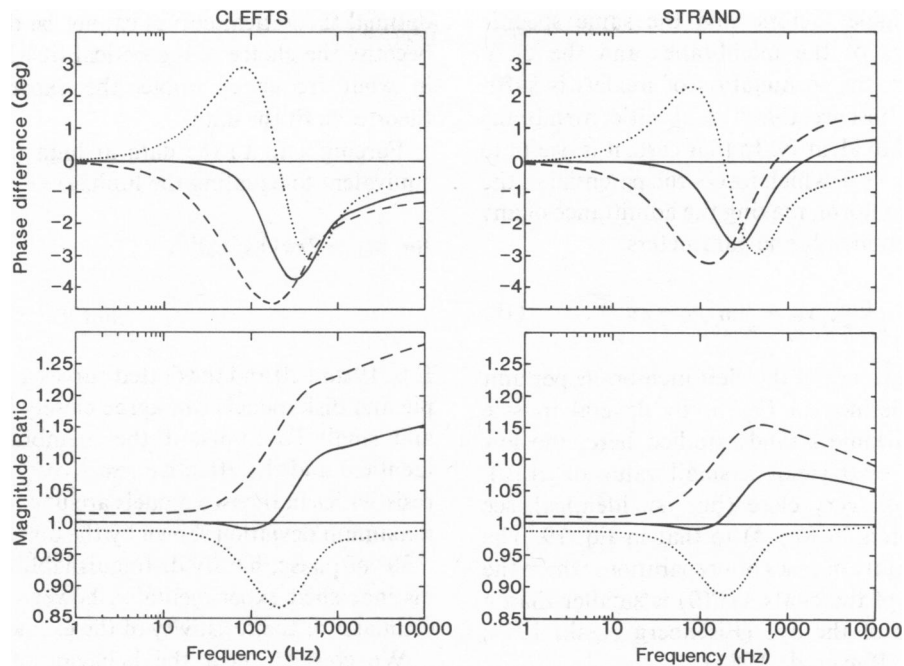
FIGURE 4   A comparison of the impedance of the pie and disk models. The *right* panels show the difference in phase angle (pie model − disk model) and the ratio of the magnitude (pie model ÷ disk model) of the impedance $Z(x, j\omega)$ of the strand. The *left* panels show the difference and ratio for a strand composed entirely of clefts, i.e., with $y_m = 0$. The dashed curves are computed for pie and disk models describing different strands, one exactly described by the pie model and one exactly described by the disk model, both with the same electrical and morphometric parameters. The dotted curves are computed for pie and disk models of the same strand (i.e., with identical morphometric and membrane parameters) forced to give nearly the same impedance at very low and very high frequencies. The value of the magnitude ratio (· · · · and ----) at low frequencies reflect the different DC resistance of the models, with these parameters. The solid curves (———) are computed for pie and disk models of the same strand are forced to give the same impedance at very low and intermediate frequencies. The parameter values used to compute these curves are essentially the average values shown in Tables II and III.

The values of G_w and C_w reported in Tables I and II are in fair agreement with the values reported by Hellam and Studt (1974a, b), Schoenberg and Fozzard (1979), and earlier workers. The mean values of the parameters estimated with the two models were essentially the same except for the estimate of the resistivity of the solution within the clefts. The resistivity estimated with the pie model was $R_{ep} = 41$ Ω-cm, whereas that estimated from the disk model was $R_{cd} = 59$ Ω-cm. The ratio of these estimates is 1.4, within the range expected from the theoretical discussion presented later. The estimate of resistivity, in any model, is linearly related to the estimate of the morphometric parameter (V_c/V_F) and so morphometric estimates must be quite accurate if the values of R_{ep} and R_{cd} are to be used to choose the best model.

Morphometric Parameters

The estimates of the specific electrical parameters previously given depend on the availability and accuracy of the morphometric measurements of V_c/V_F, S_c/V_F, ξ_s, and ξ. We use the following parameters taken or calculated from Mobley and Page (1972) as described in Levis, 1981: $S_c/V_F = 3,900$ cm²/cm³; ξ_s, the wiggle factor for the surface membrane, is taken as $\xi_s = 1.35$; and the wiggle

factor ξ for the cleft membrane is taken as $\xi = 1.8$. These values are in reasonable agreement with the estimates of Hellam and Studt, 1974a, b). The value of V_c/V_F can be related to the average width of the cleft using Eq. 9:

$$w = 2 \frac{(V_c/V_F)}{(S_c/V_F)}. \tag{18}$$

The volume fraction reported by Mobley and Page (1972) $V_c/V_F = 2.3 \times 10^{-3}$ implies a cleft width of some 12 nm, much less than the average width of 41 nm measured by Hellman and Studt (1974a, b) and outside the range of widths (20–30 nm) reported by Sommer and Johnson (1968).[4] We adopt the value $w = 30$ nm, implying $V_c/V_F = 5.9 \times 10^{-3}$, while we await more accurate measurements from our stereological colleagues.

COMPARISONS OF MODELS

Quantitative comparison of the impedance of models of the same strand clearly requires both models to use the same parameter values, the same volume of the extracellular

---

[4]Eisenberg and Cohen (1983) describe the elaborate sampling procedures needed to make reliable estimates of tiny volume fractions.

space, the same wiggle factors, and the same specific electrical parameters of the membranes and the cleft. Sometimes, however, the formulation of models is sufficiently complex or obscure that the specific membrane parameters are hard to identify. In that case, it is useful to consider the limit $R_e \rightarrow 0$, which forces the potential in the clefts to be radially uniform, making the admittance of any model depend only on membrane parameters:

$$\lim_{R_e \rightarrow 0} y_{cd} = \lim_{R_e \rightarrow 0} y_{cp} = \lim_{R_e \rightarrow 0} y_L = \pi a^2 \overline{Y}_w \quad (19)$$

where $\overline{Y}_w$ is the admittance of the cleft membrane per unit volume of strand, defined in Eq. 5. In skeletal muscle fibers, or in the Purkinje strands studied here, the low frequency limit $j\omega \rightarrow 0$ yields a small value of $a\Gamma(0)$, thereby giving a limit very close (but not identical, see lowest frequency points in Fig. 4) to that in Eq. 19. The limits differ significantly in cases or preparations where the DC length constant of the clefts $1/\Gamma(0)$ is smaller than a radius, like the lens of the eye (Eisenberg et al., 1979; Mathias et al., 1979; Rae et al., 1982).

Consider now the relation of the radial resistance in the pie and disk models. A unique relationship exists between the radial resistance of the pie and disk models only if we compare two different strands of different topological structure, one of which is exactly described by the disk model and the other by the pie model. In the strand for which the pie model is the exact description, all the clefts will conduct radial current; but in the other strand, for which the disk model is the exact description, only one-half of the clefts will conduct radial current (see Mathias et al., 1977, Fig. 2; Mathias, 1983). Hence, physically we expect (as shown by Eqs. 7, 8, and 11) the effective cleft resistivity estimated with the disk model to be twice the effective luminal resistivity estimated with the pie model, namely $r_{ed} = 2r_{ep}$, even though the actual cleft resistivities in the two models are identical, $R_{ed} = R_{ep}$.

The dashed curves in Fig. 4 compare the impedance of strands with equal membrane and morphometric parameters, with the resistivities $R_{ed} = R_{ep}$, and thus with the effective resistivities $r_{ed} = 2r_{ep}$. The models differ in the frequency band from 10–1,000 Hz, but the difference is probably too small to be experimentally convincing.

This unique comparison of different strands does not correspond, however, to our experimental situation. Rather, we are confronted with the problem of choosing the better of two imperfect models, both of which have the same wiggle factors and volume fraction of extracellular space, but with unknown specific electrical parameters. In this situation, there can be no unique theoretical relationship between the cleft resistance of one model and the other. Neither model describes the real preparation exactly, nor does it describe the electrical properties exactly. The theoretical curves produced by each model will differ from the experimental data and each other. The

optimal theoretical curves cannot be determined uniquely because the choice of theoretical fit will depend on where, in what frequency range, the experimenter forces the theories to fit the data.

Forcing a fit to the data at high frequencies is nearly equivalent to equating the limits $\omega \rightarrow \infty$:

$$\lim_{\omega \rightarrow \infty} y_{cp} \rightarrow 2\pi a(\overline{Y}_w/r_{ed})^{1/2};$$

$$\lim_{\omega \rightarrow \infty} y_{cd} \rightarrow \pi a(\overline{Y}_w/r_{ep})^{1/2}. \quad (20)$$

Eqs. 19 and 20 and the dotted curves in Fig. 4 show that the pie and disk models can agree closely in both the large Γa and small Γa limits, if the membrane parameters are identical and the effective resistivity $r_{ed} = 4r_{ep}$; i.e., if the resistivities in the two models are unequal, $R_{ed} = 2R_{ep}$. The maximum deviation shown by the dotted curves in Fig. 4 is <30° of phase, hardly distinguishable. The models can be distinguished experimentally, however, by their differing estimates of the resistivity of the extracellular space.

We consider next the behavior of the models in an intermediate range of frequencies, in which a lumped circuit is also a reasonable approximation, by expanding the admittance in a power series in the normalized radius Ga (see Hodgkin and Nakajima, 1972; Mathias et al., 1977, 1981):

pie model
$$\frac{1}{y_p} = \hat{r}_{ep} + \frac{1}{\pi a^2 \overline{Y}_w} + \dots ;$$

$$\hat{r}_{ep} = \frac{r_{ep}}{3\pi} = \frac{\xi^2 R_{ep}}{3\pi(V_c/V_F)} \quad (21)$$

disk model
$$\frac{1}{y_d} = \hat{r}_{ed} + \frac{1}{\pi a^2 \overline{Y}_w} + \dots ;$$

$$\hat{r}_{ed} = \frac{r_{ed}}{8\pi} = \frac{\xi^2 R_{ed}}{4\pi(V_c/V_F)} \quad (22)$$

where the circumflex indicates the lumped access resistance for each model and R_{ed} and R_{ep} are the (possibly different) estimates of the resistivity in the disk and pie models. If the resistivities in the two models R_{ed} and R_{ep} differ by a factor of 4/3 (with the membrane parameters, wiggle factors, and volume fractions equal), then the lumped access resistance for the models will be equal, namely $\hat{r}_{ed} = \hat{r}_{ep}$. The impedance predicted then agrees closely in the low and intermediate frequency range (see solid curves in Fig. 4). Clear differences occur only at very high frequencies, frequencies that lie beyond our measurement capability and are not shown in the figure.

Radial Distribution of Potential

Fig. 5 illustrates the theoretically predicted spatial distribution of potential in the clefts resulting from a step of potential across the surface membrane from the resting
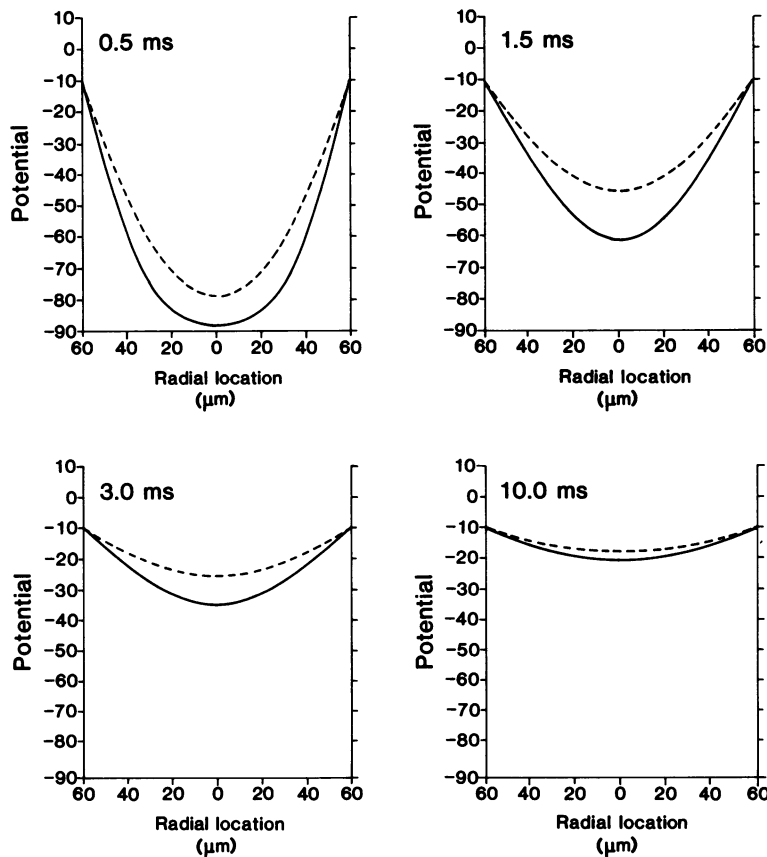
FIGURE 5 The radial distribution of potential in the disk and pie models with linear properties. The plots show the radial variation of potential computed for the parameters given in the text at the times indicated in each panel. In a real strand, the membrane parameters would change drastically with depolarizations this large; the linear case illustrated here is useful for comparison with the nonlinear simulations shown in other figures. (——) Disk model, R_{cd} = 58 Ω-cm. (---) Pie model, R_{cp} = 42 Ω-cm.

(and holding)[5] potential of −90 mV to the depolarized potential of −10 mV. We artificially assume that the strand retains its resting properties at −10 mV to allow easy comparison with simulations of nonlinear active properties. The decrement of potential along the clefts is, as expected, most severe at short times, when large capacitive currents flow through the cleft membrane shunting the radial flow of current in the clefts. The pie model predicts a more positive potential (less decrement) than the disc model at all times. (The parameters used in this simulation are specified in the Simulations section of the paper.)

Conclusion

We conclude then that the pie and disk models cannot be distinguished by their fit to our impedance data; perhaps they can be distinguished by their estimates of luminal resisitivity, by measurements of the radial distribution of

---

[5]We set the equilibrium potential and (constant) conductance of the leakage pathway so the resting potential equaled −90 mV, the desired holding potential. The leakage current in the passive case is zero; in the active case it balances the net current through the other pathways.

potential, or by morphological measurements of the radial distribution of membrane area.

SIMULATIONS

The electrical properties of the clefts of Purkinje strands limit the interpretation of voltage clamp experiments (Johnson and Lieberman, 1971; Attwell and Cohen, 1977; Schoenberg and Fozzard, 1979; Haas and Brommundt, 1980). For that reason, we performed simulations in which the surface membrane was voltage clamped (i.e., held at the command potential at all times and locations) and the cleft membrane was modeled as a nonlinear membrane embedded in the electrical and morphological structure measured and analyzed in the rest of this paper. Our simulations differed from earlier work in several ways. They included measured values of the linear parameters; they explicitly compared the disk and pie models, each with the appropriate linear and morphometric parameters; and they included the effects of electrodiffusion in the clefts, namely changes in the concentration of calcium and potassium ions in the cleft (and sarcoplasm) resulting from ionic current flux across the cleft membranes and radial electrodiffusion in the clefts.

The linear parameters used in these simulations were the resting membrane resistance R_m = 18 kΩ-cm^2, C_m = 0.9 μF/cm^2, (S_c/V_F) = 3,900 cm^{-1}, V_c/V_F = 5.9 $\times$ 10^{-3}, ξ^2 = 3.2, τ_d = 0.14, τ_p = 0.28, the resistivity of the solution in the clefts in the disk model R_{ed} = 59 ohm-cm, and the resistivity of the solution in the clefts in the pie model R_{ep} = 41 Ω-cm. Note that these are specific parameters: membrane parameters are referred to as the unit area of the membrane in which they arise, and estimates of the resistivity of the solution in the clefts are directly comparable with measurements of bulk resistivity. The morphometric parameters imply that the cleft membranes have 11.7 cm^2 of area for each 1 cm^2 of smooth surface membrane in a strand of 60 μm radius. Because the surface membrane is folded, by a factor of ~ξ_s^2 = 1.8, the cleft membranes have a total (folded) area of ~6.5 cm^2 for each 1 cm^2 of folded surface membrane.

Sodium Current

These simulations were performed with a representation of the sodium current taken from Adrian et al. (1970) for frog skeletal muscle, scaled to a temperature of 10°C with a Q_{10} of 2.5 to approximate the slower kinetics of mammalian cardiac sodium channels:

$$I_{Na} = \bar{g}_{Na}m^3h(U - E_{Na}) \tag{23}$$

where U is the potential across the cleft membrane defined in Eq. A3 and

$$\alpha_m = \frac{0.022(U + 42)}{1 - \exp[-(U + 42)/10]};$$

$$\beta_m = 0.19 \exp[-(U + 42)/18] \tag{24}$$

$$\alpha_h = 0.0014 \exp[-(U + 14)/20];$$

$$\beta_h = 0.31/[1 + \exp[-(U + 41)/10]] \tag{25}$$

where $\bar{g}_{Na}$ = 23 mS/cm^2. This value is taken from the work of Ebihara and Johnson (1980) and Ebihara et al. (1980) for chick heart; it exceeds the value used by McAllister et al. (1975) but may still be an underestimate of the true value for sheep Purkinje strands. E_{Na} was assumed to be 50 mV, and all potentials were measured in millivolts. These parameters produced cardiac sodium currents that were similar to those reported in mammalian cardiac cells at
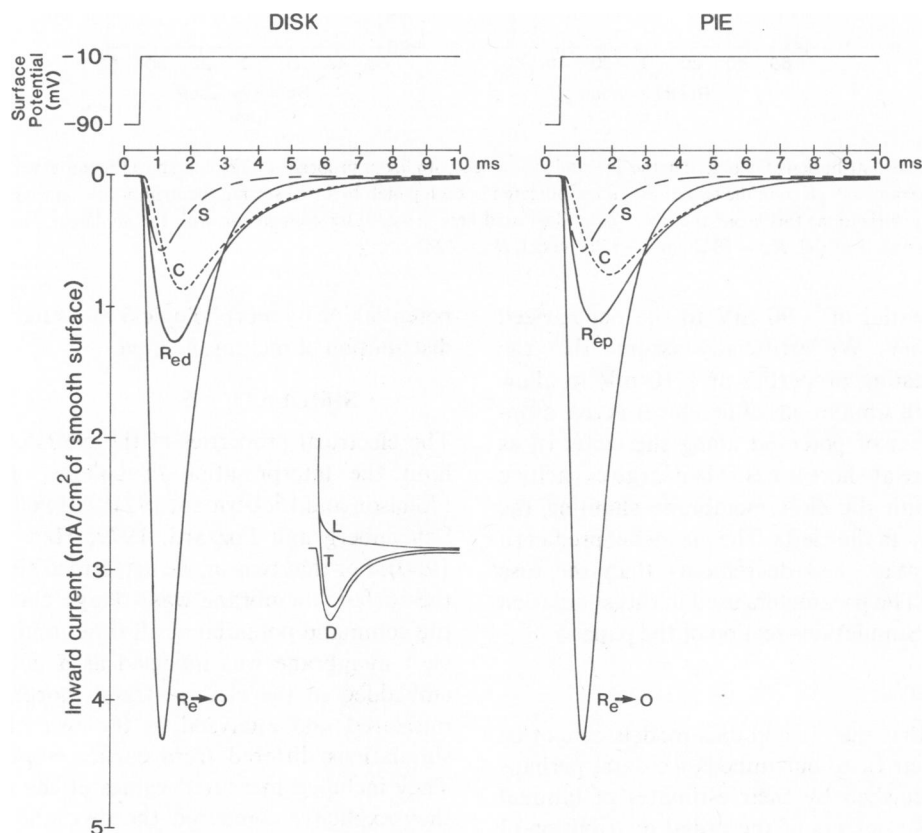

FIGURE 6 Sodium currents flowing in a simulated voltage clamp of the surface membrane of a Purkinje strand. The concentration of sodium is assumed to be constant, independent of time and location in this simulation. The *inset* shows the total current computed (*T*), the linear current that would flow if the strand parameters remained constant during a voltage step of this size (*L*), and the difference of the two currents (*D*). The panels show the sodium current across the surface membrane (*S*), the sodium current that would be measured leaving the clefts (*C*), and the total current that would be recorded under these circumstances (R_{ed} or R_{ep}). The curve labeled $R_e \rightarrow 0$ shows the current that would be recorded under ideal circumstances when there is no voltage gradient in the clefts. The drastic difference between the ideal currents and the recordable currents is explained by the lack of voltage control shown in Fig. 7.
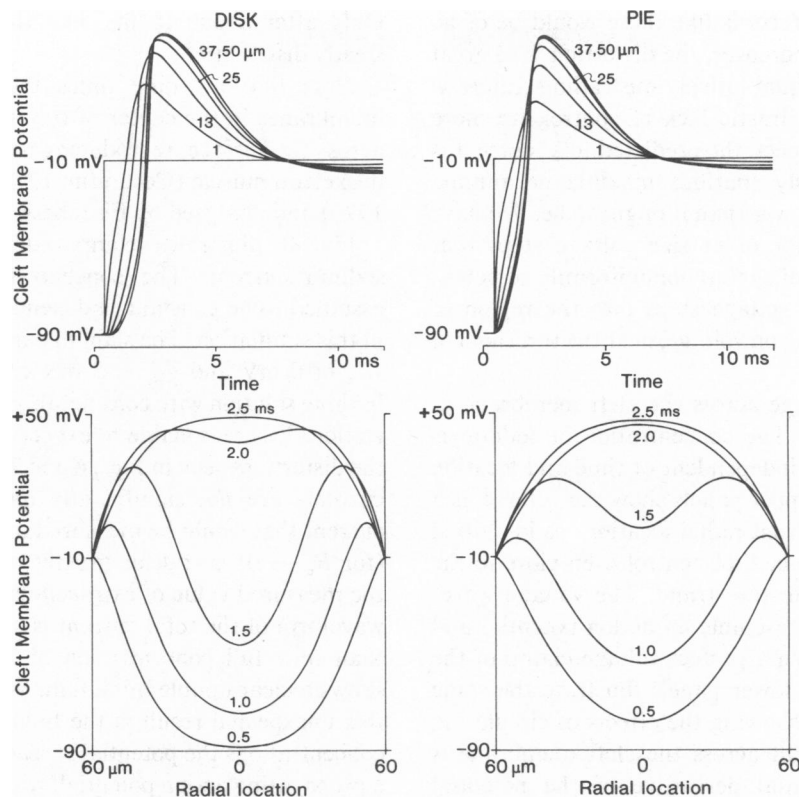
· FIGURE 7 The radial distribution of potential at short times in a voltage clamped strand with normal sodium conductance. The concentration of sodium is assumed to be constant, independent of time and location in this simulation. The upper panels show the potential across the cleft membrane, as a function of time at the depths indicated. Note that even 1 μm into the strand the potential is totally out of control, resembling a propagating action potential. The lower panels show the radial distribution of potential at different times. The slope of these curves is proportional to the radial current flowing in the clefts. Note that the radial current changes sign, indicating the existence of circulating loops of current.

some 22°C by Colatsky (1980), Brown et al. (1981), and Bodewei et al. (1982) but somewhat slower than the chick cardiac currents reported by Ebihara and Johnson (1980) and Ebihara et al. (1980) scaled by a Q_{10} of 2.5° to 22°C. Warmer temperatures, or larger or faster sodium currents would increase the spatial nonuniformity reported below.

Fig. 6 shows the sodium currents predicted using measured values of linear properties after subtraction of the linear transient as described in the inset. The concentration of sodium was assumed to be constant, independent of time and location in this simulation. The current response produced by the linear properties of the system (marked with an L in the inset to Fig. 6) was computed for a depolarizing step from −90 mV (holding potential) to −10 mV. The total current produced by the strand (with its full set of linear and nonlinear properties) is marked with a T. The difference of the two currents is marked with a D. The subtraction procedure was meant to remove the current that flows because of the linear properties of the cleft membranes. The subtraction procedure has inherent problems, although it is widely used experimentally: if the distribution of potential within the clefts is different in the two cases, for whatever reason, the subtraction will not correctly remove the linear current.

Fig. 6 shows the response of both models, for the sake of completeness. The dotted lines, marked with S, are the sodium currents computed for the surface membrane, which is presumed to be perfectly voltage clamped, with the voltage held at the constant value of −10 mV at all times. The solid lines marked with an $R_e \rightarrow 0$, are the currents computed when the extracellular resistivity is negligibly small, when the cleft membrane behaves in the voltage clamp as if it were an ideal surface membrane, with perfectly controlled transmembrane potential at all places and times. The total current in that case is a scaled version of the surface current, since we assume the specific properties of cleft and surface membrane are the same.

The total currents computed with the measured extracellular resistivities are shown as solid curves. The difference between the two curves (i.e., the difference between $R_e \rightarrow 0$ and R_{ed} or the difference between $R_e \rightarrow 0$ and R_{ep}) is an estimate of the distortion introduced by the distributed series resistance. At the peak of sodium current the amplitude is reduced by roughly a factor of 3; that is to say, the sodium current recorded in the intact strand is only some 30% of the current that would be recorded if the cleft membranes were voltage clamped with no resistance in series. Estimates of the properties of surface or cleft

membranes made from records like these would be of no quantitative use at all; moreover, the distortion is so great that they might well be qualitatively misleading. Interestingly, the signs of such drastic lack of control are more subtle than one might expect: the predicted total current is smooth, free of obviously spurious maxima or minima ("notches"), although slower than it ought to be. We have performed simulations for other size voltage steps that show the expected signs of spatial nonuniformity of potential: notches appear for voltage steps into the region of steepest dependence of g_{Na} on voltage, near the threshold of the action potential.

Fig. 7 shows the voltage across the cleft membrane at various radial locations. The concentration of sodium is assumed to be constant, independent of time and location in this simulation. The upper panels show the voltage as a function of time, at different radial locations as identified in the caption. Note the lack of control even close to the surface, some 10 μm into the strand. The voltage waveforms at greater depths resemble an action potential and are not controlled by even a perfect voltage clamp of the surface membrane. The lower panels illustrate the same data in a different way, showing the effects of circulating currents, since the current across the cleft membrane is proportional to the spatial derivative of the potential illustrated (see Eq. A2). At some times, the current is inward in some places and outward in others, forming current loops isolated from the outside world and thus unobservable and uncontrollable in the voltage clamp.

Only after about 10 ms does the potential settle to its steady distribution.

Note that at some times the depolarization of the membranes in the center of the strand is larger than that across the surface, reproducing a state observed indirectly in skeletal muscle (Costantin, 1970; Costantin and Taylor, 1973) and analyzed by Eisenberg and Costantin (1971).

Fig. 8 illustrates computations done with reduced sodium current. The concentration of sodium is also assumed to be constant, independent of time and location in this simulation. The sodium current was produced by an E_{Na} of 0 mV and $\bar{g}_{Na} = 5$ mS/cm^2, as should occur in a bathing solution with considerably reduced sodium concentration. It is reasonable to expect this procedure to reduce the distortions seen in Figs. 6 and 7; however, the simulated currents are not significantly more accurate. The total current that would be measured in a perfect voltage clamp (for $R_e \rightarrow 0$) is still far greater than that computed with the measured value of extracellular resistivity. Indeed, the waveform of the total current is seemingly more distorted than in a full concentration of sodium, because it now shows a clear double minimum. We suspect the reason for this unexpected result is the following: at normal sodium concentrations the potential spread in the clefts is virtually a propagating action potential, which happens to produce a total current with a time course not too different from the sodium current across the surface membrane. In reduced sodium, the potential spread is more controlled, and the coincidental resemblance is lost. Of course, the apparent
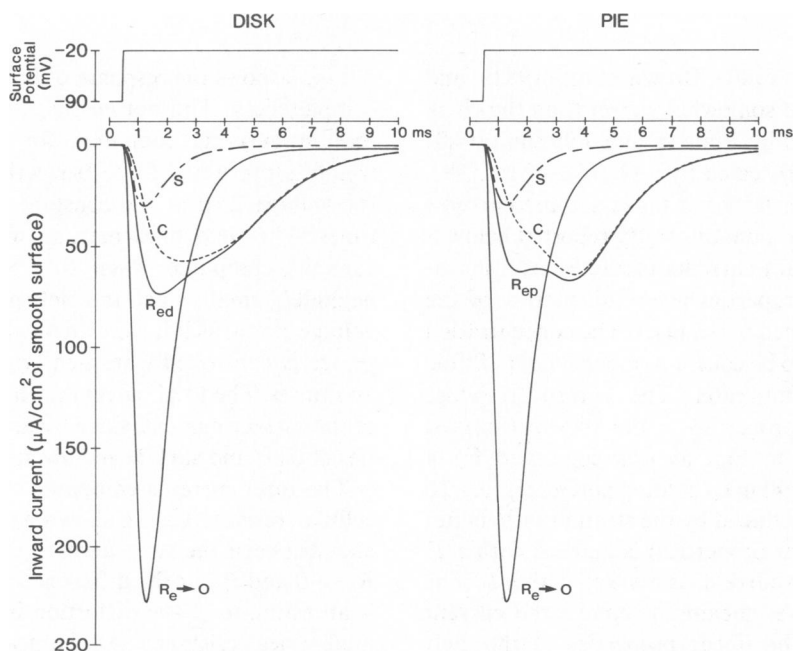

FIGURE 8 Currents flowing in a simulated voltage clamp with reduced sodium conductance and reduced equilibrium potential, as might occur in a sodium concentration 20% of normal. The concentration of sodium is assumed to be constant, independent of time and location of this simulation. The symbols are defined in the text and caption to Fig. 6. Note that the observable total currents (R_{ed} or R_{ep}) are apparently more distorted than in Fig. 6, computed with normal sodium conductance; see text for a resolution of this anomaly.

currents recorded in both situations were quite unsatisfactory approximations to the characteristics of a perfectly clamped membrane.

Fig. 9 simulates the secondary inward, predominantly calcium current, using essentially the formulation of McAllister et al. (1975) with the activation kinetics (i.e., α_d, β_d) sped up by a factor of 3 to make the currents more nearly resemble the records of Colatsky and Tsien (1979) and Ebihara and Johnson (1980) and Ebihara et al. (1980). Other formulations are possible (e.g., Drouhard and Roberge, 1982), but not worth pursuing for our purposes:

$$I_{si} = (\bar{g}_{si1} fd + \bar{g}_{si2} d')(U - E_{si}) \qquad (26)$$

where $\bar{g}_{si1} = 0.1$ mS/cm^2, $\bar{g}_{si2} = 0.01$ mS/cm^2, and $E_{si} = 70$ mV. The values of the parameters in the formulation of McAllister et al. are (when referred to 1 cm^2 of unfolded membrane)

$$d' = 1/\{1 + \exp[-0.15(U + 40)]\};$$

$$\alpha_d = 0.006(U + 40)/\{1 - \exp[-(U + 40)/10]\} \qquad (27)$$

$$\beta_d = 0.6\exp[-0.1(U + 40)]; \qquad \alpha_f = 10^{-3}\exp[-(U + 60)];$$

$$\beta_f = 0.02/\{1 + \exp[-0.1(U + 26)]\}. \qquad (28)$$

These calculations imply that the radial decrement in potential within the clefts does not seriously distort the secondary inward current of sheep Purkinje strands, although careful examination of the simulations (at a higher sweep speed than illustrated) shows that the peak current was delayed by ~5 ms. The sizes of the secondary inward currents shown in Fig. 9 are similar to the reduced sodium currents previously computed (Fig. 8), yet the spatial control is much worse in the latter case. This result suggests that the rate of change of the current is an important factor in determining the spatial uniformity of potential across the cleft membrane and thus the quality of the voltage clamp data.

Simulations of Variation of Chemical Potential

Approximations (see Eq. 16) and analysis of lumped models of the clefts of Purkinje strands (e.g., Attwell et al., 1979) suggest that the concentration of potassium should vary when physiological currents flow through the cleft membrane, just as the concentration of potassium varies in the tubules of skeletal muscle (Adrian and Freygang, 1962a). Furthermore, experimental work (e.g., Baumgarten et al., 1977, and Kline and Kupersmith, 1982; see the review of Cohen and Kline, 1982) indicates the significance of such effects. For that reason, we have performed simulations using a distributed model of the clefts and measured values of the linear electrical properties of the preparation. Our simulations allowed a radial variation in cleft concentration, potential, current flow, and membrane flux, but did not include the effects of active transport systems, exchange mechanisms, or specific binding within the sarcoplasm. Such effects are undoubtedly of considerable significance and must be included, once sufficient experimental data are available, if one seeks a quantitative analysis of the variation of chemical potential. Our goal, however, is more limited: we seek to show that the variation of chemical potential in the clefts is significant in sheep Purkinje strands under a variety of conditions.

As expected from our simulations of purely electrical phenomena, the radial decrement in electrical potential was found to be small during the flow of potassium and
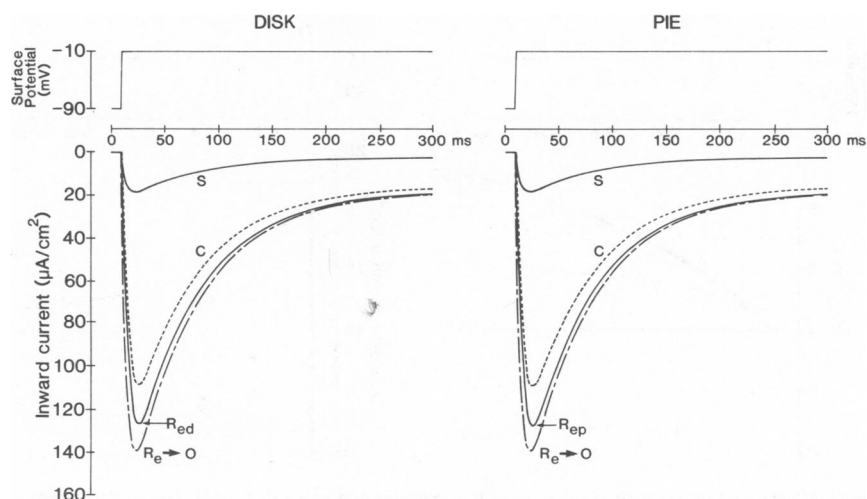

FIGURE 9 Currents flowing at long times in a simulated voltage clamp of the secondary inward current, using the McAllister et al. (1975) representation of the current. Calcium concentrations are assumed constant, independent of time and location. The symbols are defined in the text and caption to Fig. 6. Note the close resemblance of the experimentally observable currents (marked with an R_{ed} or R_{ep}) and the ideal currents (marked with an $R_e \rightarrow 0$).

calcium currents, because of the small magnitude and slow time course of these currents. The radial decrement of concentration was found to be small as well, except in the outermost region of the clefts near the surface of the strand (see Figs. 10–12). This result suggests that a lumped model of a "restricted extracellular space" (Adrian and Frey-grang, 1962a; Attwell et al., 1979) might be adequate for the sheep strand if the parameters of the lumped model are chosen by an explicit limiting process applied to the distributed model of electrodiffusion, analogous to the limiting process defined in Eqs. 19–22. The adequacy of such a lumped model needs to be investigated separately for each ionic current in each preparation.

Fig. 10 shows the concentrations of potassium (left-hand panel) and the currents (right-hand panel) expected during a prolonged voltage clamp in which potassium ions can accumulate (lower panels) or deplete (upper panels) in the clefts between cells. The sodium pump, and other transport

and binding mechanisms, have not been included in these simulations, so the results are qualitative: they cannot be taken as quantitative predictions of the actual concentrations. The upper trace in each panel is the command voltage, the potential across the surface membrane. The depth at which each concentration is computed is shown near the curves. The right-hand panels show the current across the surface membrane (marked with an S), the total current across all the cleft membranes (marked with a C), and the total current (marked with a T), the sum of the cleft and surface currents. The current that would occur if the cleft concentration of potassium were uniform is labeled *ideal*. The computations were performed for a membrane permeable only to potassium, with a specific conductance of 56 μS/cm^2. The conductance was assumed independent of time, transmembrane potential, and potassium concentration, so our results would not depend on the poorly understood properties of the potassium channels
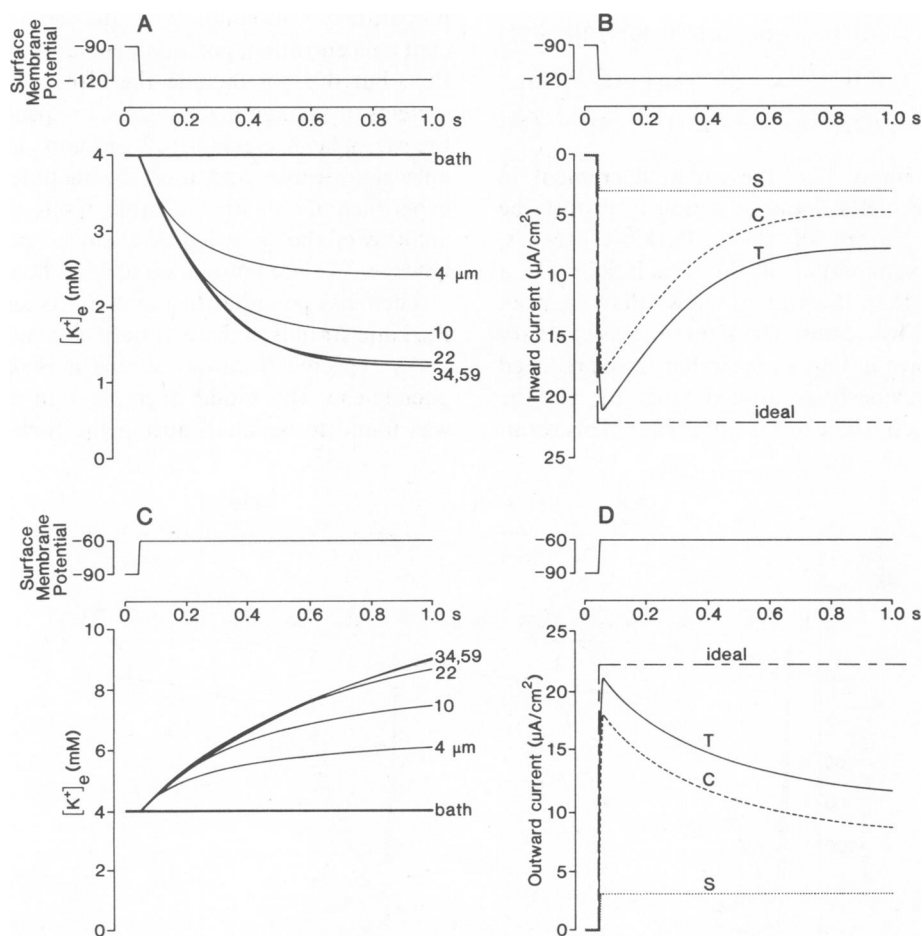

FIGURE 10   Cleft concentrations and currents of potassium with a membrane potassium conductance independent of time and potassium concentration. The step of potential applied to the surface membrane is shown at the top of each panel. The potassium concentration in the bath is 4 mM, the value used experimentally. The intracellular concentration is initially 140 mM; thus, the initial value of E_K is −90 mV. The *left* panels show the potassium concentration in the bath, in the sarcoplasm, and in the clefts at the various depths indicated. The *right* panels show the total potassium current across the surface membrane (S), the cleft membranes (C), and the total preparation (T). The curves labeled *ideal* show the current that would flow in an ideal preparation in which the concentration of potassium was constant, independent of time and location. The computation shown is for the disk model; we expect that computations for the pie model would give similar results.

and transport systems of the Purkinje strand. Our simulations thus give the time scale and magnitude expected for the changes of concentrations in the natural situation; quantitative analysis, however, requires more detailed knowledge of channel properties. Nonetheless, it is comforting that our simulations are not incompatible with the experimental results reported by, for example, Baumgarten et al., 1977, and Kline and Kupersmith, 1982.

The changes of concentration can be intuitively understood for both the hyperpolarizing and depolarizing steps in potential. The potassium concentration in the clefts will tend to equilibrate with the cleft membrane potential; that is to say, the chemical potential (i.e., the the equilibrium potential) for potassium will approach the cleft membrane potential at any radial location. The time course of the concentration changes reflects the amount of concentration change necessary to equilibrate the chemical potential and the electrical potential. Thus, the response to the hyperpolarizing step will be faster than the response to the depolarizing step because the change in concentration required is smaller. When the hyperpolarizing step is applied, the chemical potential must eventually approach −120 mV, corresponding to a change in cleft concentration of 2.8 mM potassium. When the depolarizing step is applied, extracellular potassium must eventually approach 12.9 mM, corresponding to a change of 8.9 mM.

Other simulations of potassium movements were per-

formed using a more complex description of the potassium channel (Eqs. 1 and 2 of Noble, 1965) allowing the potassium conductance to vary with voltage and concentration. These simulations showed changes in concentration on a similar time scale but a maximum in the plot of cleft current vs. time appeared in the response to a depolarizing step of potential. Such a biphasic current might traditionally be interpreted as two components reflecting flux through two different channels. If the clefts of cardiac muscle contained potassium channels with the complex properties of the inward rectifier of skeletal muscle or starfish oocytes (steep negative slope conductance and dependence on extracellular potassium [Spalding et al., 1981], independence of intracellular potasssium but dependence on intracellular sodium [Hagiwara and Yoshii, 1979], apparent time dependence [Leech and Stanfield, 1981]; see general analysis of Hille and Schwartz, 1978), the potassium current might well have multiple maxima and thus seem to have multiple components, even if just one channel were involved.

The next set of simulations shows the concentration changes and calcium currents, described by the secondary inward conductance, expected in response to a prolonged depolarizing step in potential for two cases. In these simulations the calcium conductance is described by Eqs. 26–29 with $\bar{g}_{si1} = 0$ and $\bar{g}_{si2} = 0.1$ mS/cm^2. The effects of calcium pumps, exchange mechanisms, and specific bind-
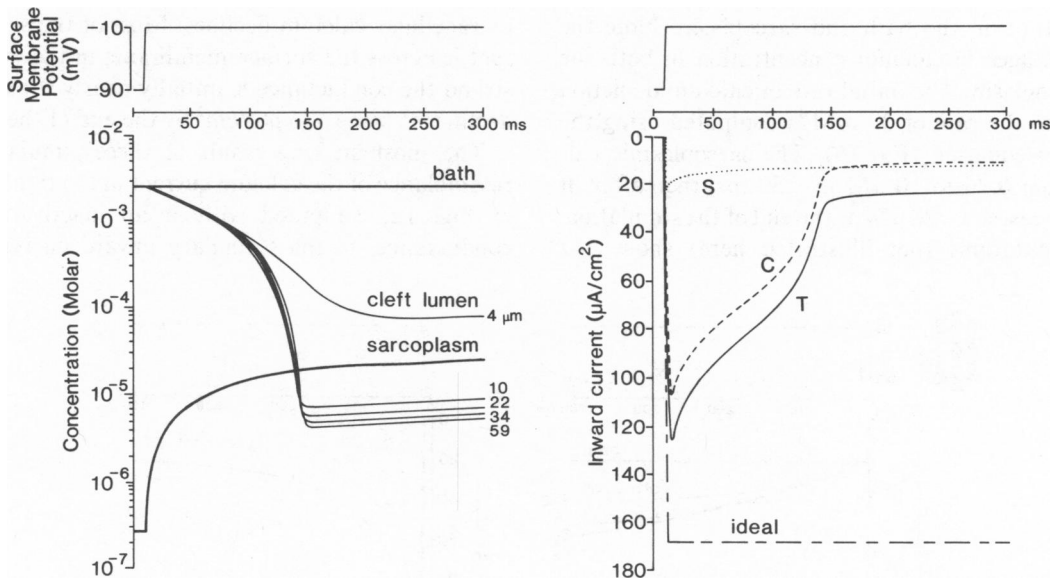

FIGURE 11 Cleft concentrations and currents of calcium with a membrane calcium conductance independent of time and calcium concentration. A step of potential of −10 mV from a resting potential of −90 mV is applied to the surface membrane. The calcium concentration in the bath is 2.7 mM, the larger value used experimentally. The intracellular concentration is initially 0.26 μM; thus, the initial value of E_{si} is about +115 mV. The *left* panel shows the calcium concentration in the bath, in the sarcoplasm, and in the clefts at the various depths indicated. Note the hundredfold changes in concentration during the depolarizing step. The *right* panel shows the calcium current across the surface membrane (*S*), the cleft membranes (*C*), and the total preparation (*T*) are also shown. Note that the current turns off even though the calcium conductance used in the simulation did not include an inactivation process. The curve labeled *ideal* is the total current in an ideal preparation, in which the electrochemical potential across all the membranes was controlled at a constant value. The initial peak of the total current (*T*) does not coincide with the ideal line because of the large initial voltage nonuniformity in the clefts. The computation shown is for the disc model; we expect that computations for the pie model would give similar results.

ing are not included in this simulation, because of lack of data. Thus, the results are essentially qualitative and cannot quantitatively predict the concentration changes in the clefts.

In Fig. 11 the calcium conductance, defined in Eqs. 26 and 27, depends on voltage but is strictly independent of time and calcium concentration. In Fig. 12, however, the calcium conductance depends on calcium concentration in a passive (diffusionlike) manner, varying nearly linearly with extracellular Ca_e when $Ca_e \gg Ca_i$ (see Eq. 29). In this case, the conductance varies with time, but only because calcium concentration varies:

$$\bar{g}_{si2} = P_{si} \frac{Ca_e - Ca_i}{\ln (Ca_e/Ca_i)} \tag{29}$$

where P_{si} is a constant permeability factor chosen to produce the initial values of $\bar{g}_{si2}$ = 0.1 mS/cm² already mentioned. This equation was derived from Sten-Knudsen (1978, Eq. 124 and the unnumbered equation on p. 85). We assume that the secondary inward current is entirely carried by calcium ions and in this simulation we assume the concentrations of potassium and sodium to be constant, independent of time and location. Current carried by other ions through this channel (e.g., sodium, Reuter, 1979) would quantitatively modify our results but not change our conclusions.

The left-hand panel of Fig. 11 shows the concentration of calcium in the clefts at the various depths indicated and the concentration in the bath and sarcoplasm. Note the very large changes in calcium concentration in both the cleft and sarcoplasm. The initial rate of calcium depletion is very close to the rate of 33 mM/s computed using the approximation equation (Eq. 16). The sarcoplasmic calcium rises from 0.26 to 10 μM in <50 ms; thereafter, it gradually increases to ~20 μM at the end of the simulation. Further computations (not illustrated here) show that

qualitatively similar changes occur in the cleft if the sarcoplasmic concentration is held constant.

The right-hand panel of Fig. 11 shows calcium currents across the surface membrane (marked with an S), across the cleft membrane (marked with a C), and across both membranes (marked with a T), under these conditions. The current labeled *ideal* is that which would flow if the calcium concentration in the clefts and sarcoplasm did not vary. The initial rapid falling phase of the calcium current is primarily caused by the intracellular accumulation of calcium, as can be seen by comparing the time course of current and the time course of intracellular calcium concentration. The final rapid falling phase of calcium current is due to the progressive depletion of extracellular calcium. The rate of change of extracellular calcium concentration with time does not vary much during most of the simulation; rather the change becomes progressively more important as the calcium concentration becomes less. During this time period the gradient of electrochemical potential for calcium approaches zero as the extracellular and intracellular concentrations equilibrate with the membrane potential.

Fig. 12 includes the dependence of calcium conductance on concentration as just described. The concentration changes more gradually with time than Fig. 11. The initial rapid decline in current is again produced by the rapid intracellular accumulation of calcium. The overall time course is influenced by accumulation, depletion, and the decline in calcium conductance as the concentration of extracellular calcium declines. Most of the sustained current is across the surface membrane; in the middle of the strand the conductance is initially nearly 0.1 mS/cm² but declines to some 5–6 μS/cm² by the end of the simulation.

The most striking result of these simulations is the resemblance of the calcium current in the right-hand panel of Fig. 12, computed without an inactivating calcium conductance, to the secondary inward current shown in
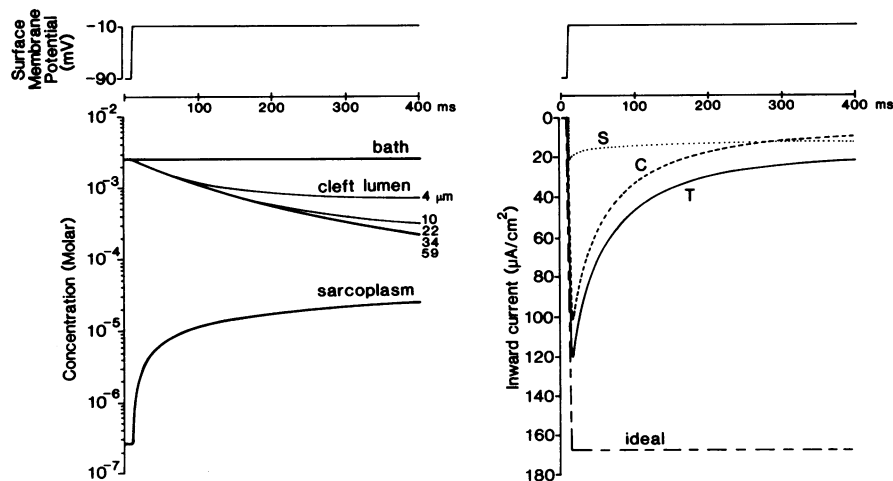

FIGURE 12 Cleft concentrations and currents of calcium with a membrane calcium conductance which depends on the concentration but not time. See caption of Fig. 11.

Fig. 9, which resembles experimental records. Further simulations were performed to check this result: inclusion of an inactivating calcium conductance in the membrane (Reuter et al., 1982) or a constant calcium concentration in the sarcoplasm did not qualitatively alter the large changes in calcium concentration and the resulting changes in calcium current.

Our simulations do not include some potentially important properties of the calcium channel; for example, the time course and amplitude of the secondary inward conductance g_{si} is probably inadequately described by either of our formulations. Furthermore, when intracellular calcium concentration varies substantially, there may be direct effects on its own conductance, including a concentration-dependent inactivation of the conductance (Eckert et al., 1981; Marban and Tsien, 1981), more extensive than the concentration dependence described by Eq. 29. Intracellular calcium must also be expected to have specific effects on the conductances for other ions as well because the conformation of such channels is dependent on a divalent binding site (Gilly and Armstrong, 1982a, b). Finally, our simulations ignore the significant amounts of sodium ions (and perhaps other ions as well) likely to flow through the calcium channel (Reuter, 1979). If sodium ions were only 1% as permeable as calcium, they would carry some one-third of the current, quantitatively modifying our results.

Despite these simplifications in our description of the calcium channel, one conclusion seems inescapable. Variations in the gradient of calcium concentration will have large effects on the turn off of calcium current in both the voltage clamp and the cardiac action potential.

DISCUSSION

Comparison of Models

Uncertainties in our results arise primarily from limitations in the bandwidth of our electrical measurements and inadequacies in the available morphological information. If the morphology of an average Purkinje strand were known in sufficient detail, the choice of circuit model for the ensemble could be made by studying the radial distribution of clefts. If the topology and morphometric parameters of cleft and outer membrane were known for each Purkinje strand, the circuit model appropriate for that strand could be synthesized numerically, using the methods of Mathias (1975) or perhaps analytically using the methods of Mathias et al. (1977) and Levin and Fozzard (1981).

In any case, electrical measurements made in the cytoplasm of the myocytes are unlikely to distinguish between models. Simulations suggest, however, that measurements of the distribution of potential in the cleft could distinguish between models. In skeletal muscle fibers, the spatial distribution of tubular potential has been estimated by Nakajima and Gilai (1980a, b) and Heiny and Vergara

(1982) using optical signals measured in fibers stained with voltage-sensitive dyes. Morad and colleagues (Morad and Salama, 1979; Morad and Weiss, 1981) have measured optical signals from cardiac preparations that might be expected to depend on the spatial distribution of potential in the clefts.

Voltage Clamp, Series Resistance, and Structural Analysis

The voltage clamp has been widely used to measure physiological current flow since its invention by K. S. Cole (see historical reviews by Hodgkin, 1976, and Cole, 1982). Most physiological conductances depend fundamentally on the voltage and concentrations of permeant ions on each side of the membrane, and thus a controlled study of physiological currents requires control of the membrane potential and concentration of permeant ions. Seeking to exploit the success of the voltage clamp of simple axonal preparations, physiologists have applied the method to preparations of considerably greater complexity (e.g., cardiac muscle [Deck and Trautwein, 1964; Hecht et al., 1964; Noble and Tsien, 1969], skeletal muscle [Adrian et al., 1970]). The voltage clamp has been less successful in these more complex preparations, particularly cardiac preparations: no one knows if the disconcerting number of reported currents reflects a variety of different channels or is an artifact of the complex structure of cardiac tissues (or both).

Even in the squid axon, structural complexity can produce significant problems. Potassium ions accumulate in the periaxonal space between axon membrane and Schwann cell, as first reported by Frankenhaeuser and Hodgkin (1956) and most recently analyzed by Taylor et al. (1980). The resistance in series with the membrane, arising in part in the periaxonal space, limits the speed and reliability of the clamp because current flow through this resistance ensures that the voltage across the membrane is no longer a faithful replica of the potential commanded by the voltage clamp circuit. Preparations with complex structure must be expected to have much larger series resistance than squid axon; impedance measurements of frog skeletal muscle (originally by Falk and Fatt, 1964; later by many workers reviewed in Eisenberg, 1983) suggest that most of its membrane is in series with a resistance of some 200 Ω-cm^2, which is 50–100 times larger than for a squid axon. A reasonable conclusion from the impedance measurements, voltage clamp measurements (Adrian et al., 1970), and simulations (Adrian and Peachey, 1973) of frog skeletal muscle and cardiac muscle (Schoenberg and Fozzard, 1979; Haas and Brommundt, 1980) is that interpretation of voltage clamp measurements in the presence of this much series resistance requires detailed independent experimental evidence describing the equivalent circuit of the preparation.

As expected, our experiments showed that almost all the resistance in series with the membranes of Purkinje strands

was distributed; the amount of lumped resistance in series with the surface membrane was negligibly small compared with the amount of distributed resistance in series with the cleft membranes. This finding has important consequences for voltage clamp experiments. It implies, for example, that compensation of series resistance must be undertaken with great caution. The feedback method (Hodgkin et al., 1952) or the chopped clamp method (Brennecke and Lindemann, 1974a, b; Wilson and Goldner, 1975; Goldman and Morad, 1977; Merickel, 1980) can successfully compensate for lumped series resistance. But that resistance is trivial in sheep Purkinje strands compared with the distributed series resistance of the cleft. Compensation for the distributed series resistance of the cleft is impossible because the different pieces of cleft membrane are at different potentials as long as concentration gradients or current flow exists in the clefts.

The measurements and simulations presented here confirm the conclusions of earlier simulations (Schoenberg and Fozzard, 1979; Haas and Brommundt, 1980) that measurements of sodium currents from sheep Purkinje strand are likely to be incorrect, even if they appear as expected. Other preparations with similar structural complexities and similar linear properties (e.g., ventricular or atrial myocaridum, skeletal muscle) must be expected to have similar distortions in their current records.

Our measurements and simulations also suggest that radial control of electrical potential is unlikely to be an overwhelming problem in the measurement of the the slower currents important during the plateau of the action potential. The control of the chemical potential (i.e., the concentration gradient) across the membranes is quite a different matter.

Electrodiffusion in Cardiac Preparations

Our simulations showed a substantial variation of the chemical potential of calcium and potassium, arising from the flux of the ions across the cleft membrane and the radial electrodiffusion of the ions in the clefts. A simplified version of Eq. 16 is useful in evaluating the size of these effects, particularly in different preparations:

$$\text{initial } \frac{d}{dt} [x] \simeq 0.01 \frac{2g_x}{zw} (U - E_x). \tag{30}$$

Here the rate of change of $[x]$ is in mM/s; w is the width of the cleft, in centimeters (see Eq. 18); g_x is the conductance (S/cm^2) of unfolded membrane; U is the electrical potential across the cleft membrane, in millivolts; E_x is the equilibrium potential for ion x (of charge z); the factor 0.01 reconciles chemical and electrical units and has dimensions (mol/liter)/[C/(cm^3-s)].

The intracellular accumulation and extracellular depletion of calcium predicted by the simplified equation is close to that shown in the full scale simulation (see Figs. 10 and 11) and is large enough to shut off calcium current (as

seems to be the case in skeletal muscle [Almers et al., 1981]), even if the conductance for calcium did not inactivate. The current would decline even if the conductance were maintained because the depletion of calcium in the clefts and the accumulation of calcium in the sarcoplasm removes the gradient of chemical potential that drives the calcium movement.

The implications of such large effects are substantial, and so one should consider its generality. Eqs. 16 and 30 provide simple approximate estimates of the initial rate of change of concentration, and the results shown in Fig. 11 show that the approximation is quite accurate. Obviously, the larger the cleft width, the smaller the effect; but our approximate expressions show that even in clefts of substantial width, such as those of dog Purkinje strands (see Tables 3 and 4 of Eisenberg and Cohen, 1983) significant changes in concentration would occur in the hundreds of milliseconds of the cardiac action potential.

When considering other preparations, with more non-uniformity of cleft structure than sheep Purkinje strands, one must remember that the smallest clefts dominate the electrochemical properties, whereas the largest clefts dominate estimates of morphometric parameters. Mathias et al. (1981a, c), show that substitution of average morphometric parameters into equations like the disk model underestimates the contribution of clefts to the electrical properties of the tissue. Thus, the electrochemical effects of the narrowest clefts are likely to be substantial, even in preparations like dog Purkinje strand, which have less of these narrow clefts than sheep Purkinje strands.

We must also consider the details of our analysis to be sure the assumptions made do not invalidate its significant conclusions. The equations we use to describe flow in the clefts are in themselves somewhat simplified, since they ignore coupling between flows of ions, on the one hand, and convection due to osmotic effects, on the other. Only the largest concentration changes for potassium are likely to be influenced significantly by such effects.

More serious is our simplification of the properties of cardiac membranes. We have ignored the contributions of active transport systems because of lack of knowledge, not because we doubt their role. We have also used descriptions of the channel conductance that do not vary realistically with the electrical or chemical potential. More complete descriptions of cardiac calcium and potassium channels are not available, in part because most measurements have been contaminated by radial variation in the electrochemical potential within the clefts.

Our assumptions concerning the sarcoplasm of cardiac cells are also important. Cardiac sarcoplasm includes many systems that modify the concentration of calcium ions: several calcium-binding proteins are present in substantial concentration, most notably troponin and perhaps parvalbumin (in some preparations); the sarcoplasmic reticulum has elaborate mechanisms for the release and uptake of calcium, as does the surface and presumably

cleft membrane as well (Fabiato and Fabiato, 1979). These systems will certainly modify the intracellular concentration of calcium.

The simplifications just described do not affect the main point of our analysis of ionic concentrations in the clefts. The flux of calcium and potassium across the cleft membrane is sufficiently large that realistic analysis of the cardiac action potential must include electrodiffusion of calcium and potassium in the clefts. This conclusion of our theoretical simulations is supported by recent experimental work on calcium fluxes in skeletal muscle (Almers et al., 1981) and measurements of resting calcium concentration in cardiac muscle (Marban et al., 1980), the lumped calculations of Attwell et al. (1979), and the measurements of potassium accumulation from number of studies, e.g., Baumgarten et al. (1977), Kline and Kupersmith (1982), and Cohen and Kline (1982).

Interpretation of Total Ionic Current

Our simulations of voltage clamp illustrate the importance of controlling the electrochemical potential, both the electrical potential and the concentration gradient. When sodium currents flowed, the current recorded in the voltage clamp bore little resemblance to the current through the sodium channel. When secondary inward, predominantly calcium currents flowed, the current recorded in the voltage clamp was a reasonable representation of the total ionic current through the corresponding channels, but the gradient of electrochemical potential across each channel varied with time and with the radial location of the channel. Thus, analysis of the properties of an ensemble of ionic channels must not assume a constant gradient of electrochemical potential.

Even if the electrochemical potential is perfectly controlled across cleft and surface membrane, the recorded current must be parsed into the currents through individual channels before molecular mechanisms can be reasonably studied. If the currents through different channels have similar time and voltage dependence or drug sensitivity, they probably can only be uniquely separated by physically isolating the channels, whether by patch clamp or purification and reconstitution (Coronado and Latorre, 1982).

Conclusions

The major conclusions of this paper are (a) that the linear electrical properties of sheep Purkinje strands must be described by a distributed model, in which the inner membranes and the resistance of the cleft play a major role. (b) The pie and disk models of the strands cannot be distinguished by measurements of potential in the cytoplasm; they can probably be distinguished by measurements of the distribution of potential across the cleft membranes or by direct morphological measurement of the radial distribution of cleft membrane. (c) The resistance in series with the membranes of Purkinje strands is almost all

distributed; the lumped component is small. (d) Reliable estimates of sodium current cannot be made from this preparation, even if the current is substantially reduced by experimental manipulation. (e) The electrical potential across the cleft membranes can be controlled during slower currents, such as the secondary inward, predominantly calcium current, but (f) the chemical potential of calcium and potassium ions cannot be controlled during the slower currents: the concentration of these ions changes substantially under physiological conditions, whether natural or voltage clamped, and the changes in concentration must significantly effect potassium and calcium currents. Thus, (g) either the electrical or chemical component of electrochemical potential must be expected to vary significantly in the clefts as each ionic current crosses the cleft membrane in an action potential or voltage clamp step. For sodium, the electrical potential varies; for potassium and calcium, the chemical potential varies.

APPENDIX

Description of Branched and Unbranched Clefts in Tissues and Cells of Different Geometry

Although the differential equations describing the spread of potential in clefts have often been described in the biological literature (Jack et al., 1975; Haas and Brommundt, 1980; and Levin and Fozzard, 1981), it seems worthwhile to present a unified treatment of branched and unbranched clefts in tissues and cells of different geometry, written in terms of stereological estimates of morphometric parameters and the general tortuosity factor defined by Mathias, 1983. Current flow in tissues of complex geometry has been extensively analyzed (e.g., Eisenberg and Johnson, 1970; Eisenberg et al., 1979; Peskoff, 1979). The last two of these papers mathematically establish the relationship between longitudinal and radial current flow in tissues containing clefts and tubules and show that our Eqs. 1 and 2, introduced originally by Falk and Fatt (1964), are quite accurate.

The field equations describing the spread of potential within single cells or syncytial tissues can often be simplified into transmission line equations (Eisenberg and Johnson, 1970; Eisenberg et al., 1979; Peskoff, 1979), the first a statement of conversation of current, the second a statement of Ohm's law derived from Eqs. 2 and 4 of Mathias, 1983:

$$\frac{\partial i(r, x)}{\partial r} = S_r(r)(S_c/V_F) \left[G_w U + C_w \frac{\partial U}{\partial t} + I_{ion}(U) \right] \quad (A1)$$

$$\frac{\partial U}{\partial r} = \frac{i(r, x)}{S_r(r)} \frac{R_e}{\tau(V_c/V_F)}. \quad (A2)$$

In these equations the morphometric parameters are local variables that can change with position. $U(r, x; t)$ is the potential across the cleft membrane; $U_c(r, x; t)$ is the potential in the cleft; and $V(x; t)$ is the potential in the sarcoplasm:

$$U(r, x; t) \equiv V(x; t) - U_c(r, x; t). \quad (A3)$$

The differential Eqs. A1 and A2 are completed by the boundary conditions that the current i in the middle of the preparation is finite (and thus in fact zero in a symmetrical preparation) and that the potential within the cleft U_c is zero at the perimeter of the fiber; thus, $U(a, x; t) = V(x; t)$.

TABLE III
$S_r(r)$ IN SEVERAL GEOMETRIES

Geometry	$S_r(r)$
Cylinder (disk)	$2\pi r L_x$
⟨Cylinder (pie)⟩*	$2\pi(a/2)L_x = \langle S_r(r)\rangle$
Slab	$L_y L_x$
Sphere	$4\pi r^2$

*The value of $S_r(r)$ given for the pie model is a constant, because it is a spatial average, as indicated by the brackets ⟨ ⟩, to be used with the morphometric parameters of the whole strand, as described in the Appendix.

The tortuosity factor τ is defined in Mathias, 1983. I_{ion} is the nonlinear ionic current (in amperes per square centimeter) flowing outward through the cleft membrane, including fast sodium currents, slow inward currents, and so on. i is the current (in amperes) flowing radially outward in the clefts $i = J_r(r) S_r(r)$, where J_r is the flux density used in more general treatments (Mathias, 1983). In a preparation like a strand that extends longitudinally, i is the current flowing radially in the clefts contained in a length L_x (in centimeters) of strand. $S_r(r)$ is the cross-sectional area of tissue available for radial current flow (Table III). (Note that $S_r(r)$ is the area of a cylindrical surface; it is neither the cross-sectional area of the strand nor the cross-sectional area of the clefts.) The generic coordinate r represents the direction of predominant current flow in the clefts.[6]

Eqs. A1 and A2 cannot be used until the morphometric parameters and $S_r(r)$ are explicitly described as a function of radial location. In tissues with radially uniform structure, the morphometric parameters S_c/V_F and V_c/V_F are constant and the resulting differential equation has the symmetry of the tissue. The solution to the differential equation is often easy to evaluate using the values of $S_r(r)$ given in Table III and using standard stereological estimates of morphometric parameters (Mobley and Page, 1972; Eisenberg and Cohen, 1983).

In tissues with nonuniform structure, more information is needed before the differential equations can be solved and the solutions evaluated. For example, in strands with the structure of the pie model the morphological parameters must be written explicitly as a function of radial location and the average morphological parameters available from stereological measurements. In the pie model, the local values of S_c/V_F and V_c/V_F vary as $1/2\pi r$, but $S_r(r)$ varies as $2\pi r$. Only the products of the local morphometric parameters and $S_r(r)$ appear in Eqs. A1 and A2. Thus, in the pie model the r dependence cancels and the products are independent of radial location. The product can then be written in terms of the average morphometric parameters available from stereological measurements and the average value of the area, namely $\langle S_r(r)\rangle$, as given for the pie model in Table III.

The differential equation for the pie model resulting from this procedure is of Cartesian form, with constant coefficients, despite the fact that the independent spatial variable is the radial coordinate r of a cylindrical coordinate system. The most natural representation of the solution of the cable equation for the pie model is thus written in exponentials, unlike the solution of most differential equations describing structures with cylindrical symmetry, which involve Bessel functions.

The solution to the differential Eqs. A1 and A2 determine the admittance y_c of the clefts:

$$y_c \equiv \frac{i(a, x)}{U(a, x)} = \frac{i(a, x)}{V(x)} \qquad (A4)$$

where the spatial argument a is used generically to indicate the location of the perimeter of the preparation.

---

[6]In a cylinder or sphere, r is the radial coordinate; in a thin slab, it is the coordinate ranging from one side to the other of the slab.

Peskoff (1979) has shown that the most significant link between the (radial) flow of current in the clefts and the (longitudinal) flow of current in the cytoplasm of a strand is through the admittance y_c. Eq. A4 defines that admittance in terms of the solution of the cable equation describing the radial spread of potential in the clefts; Eqs. 1 and 2 of the text introduce the cleft admittance into the cable equation describing the longitudinal spread of potential in the cytoplasm. The current through the clefts simply adds another shunt pathway, in parallel with the surface membrane, by which current can flow from cytoplasm to the outside bathing solution just as Falk and Fatt (1964) originally assumed for skeletal muscle.

REFERENCES

Abramowitz, M., and I. A. Stegun, editors. 1964. Handbook of Mathematical Functions. National Bureau of Standards, Washington, D.C. 355–434.

Adrian, R. H., and W. Almers. 1974. Membrane capacity measurements on frog skeletal muscle in media of low ion content. J. Physiol. (Lond.). 237:573–605.

Adrian, R. H., W. K. Chandler, and A. L. Hodgkin. 1970. Voltage clamp experiments in striated muscle fibers. J. Physiol. (Lond.). 208:607–644.

Adrian, R. H., L. L. Costantin, and L. D. Peachey. 1969. Radial spread of contraction in frog muscle fibres. J. Physiol. (Lond.). 204:231–257.

Adrian, R. H. and W. H. Freygang. 1962a. The potassium and chloride conductance of frog muscle membrane. J. Physiol. (Lond.). 163:61–103.

Adrian, R. H., and W. H. Freygang. 1962b. The potassium conductance of frog muscle membrane under controlled voltage. J. Physiol. (Lond.). 163:104–114.

Adrian, R. H., and L. D. Peachey. 1973. Reconstruction of the action potential of frog sartorius muscle. J. Physiol. (Lond.). 235:103–131.

Almers, W., R. Fink, and P. T. Palade. 1981. Calcium depletion in frog muscle tubules: the decline of calcium current under maintained depolarization. J. Physiol. (Lond.). 312:177–207.

Attwell, D., and I. Cohen. 1977. The voltage clamp of multicellular preparations. Progr. Biophys. Mol. Biol. 31:201–245.

Attwell, D., D. Eisner, and I. Cohen. 1979. Voltage clamp and tracer flux data: effects of a restricted extra-cellular space. Q. Rev. Biophys. 12:213–261.

Baumgarten, C. M., G. Isenberg, T. McDonald, and R. E. Ten Eick. 1977. Depletion and accumulation of potassium in the extracellular clefts of cardiac Purkinje fibers during voltage clamp hyperpolarization and depolarization. Experiments in sodium-free bathing media. J. Gen. Physiol. 70:149–169.

Bodewei, R., S. Hering, B. Lemke, L. V. Rosenshtraukh, A. I. Undrovinas, and A. Wollenberger. 1982. Characterization of the fast sodium current in isolated rat myocardial cells. J. Physiol. (Lond.). 325:301–315.

Brennecke, R., and B. Lindemann. 1974a. Theory of a membrane-voltage clamp with discontinuous feedback through a pulsed current clamp. Rev. Sci. Instrum. 45:184–188.

Brennecke, R., and B. Lindemann. 1974b. Design of a fast voltage clamp for biological membranes, using discontinuous feedback. Rev. Sci. Instrum. 45:656–661.

Brown, A. M., K. S. Lee, and T. Powell. 1981. Sodium current in single rat heart muscle cells. J. Physiol. (Lond.). 318:479–500.

Carnahan, B., H. A. Luther, and J. O. Wilkes. 1969. Applied Numerical Methods. John Wiley & Sons, Inc., New York. 1–604.

Chandler, W. K., R. F. Rakowski, and M. F. Schneider. 1976. Effects of glycerol treatment and maintained depolarization on charge movement in skeletal muscle. *J. Physiol. (Lond.).* 254:285–316.

Clausen, C., S. A. Lewis, and J. M. Diamond. 1979. Impedance analysis of a tight epithelium using a distributed resistance model. *Biophys. J.* 26:291–318.

Cohen, I., and R. Kline. 1982. K^+ fluctuations in the extracellular spaces of cardiac muscle. *Circ. Res.* 50:1–27.

Colatsky, T. J. 1980. Voltage clamp measurements of sodium channel properties in rabbit cardiac Purkinje fibres. *J. Physiol. (Lond.).* 305:215–234.

Colatsky, T. J., and R. W. Tsien. 1979. Electrical properties associated with wide intercellular clefts in rabbit Purkinje fibres. *J. Physiol. (Lond.).* 290:227–252.

Cole, K. S. 1982. Squid axon membrane: impedance decrease to voltage clamp. *Annu. Rev. Neurosci.* 5:305–323.

Coronado, R., and R. Latorre. 1982. Detection of K^+ and Cl^- channels from calf cardiac sarcolemma in planar lipid bilayer membranes. *Nature (Lond.).* 298:849–852.

Costantin, L. L. 1970. The role of sodium current in the radial spread of contraction in frog muscle fibers. *J. Gen. Physiol.* 55:703–715.

Costantin, L. L., and S. R. Taylor. 1973. Graded activation in frog muscle fibers. *J. Gen. Physiol.* 61:424–443.

Cranefield, P. F. 1975. The Conduction of the Cardiac Impulse. Futura Publishing Co., Inc., Mount Kisco, NY. 1–404.

Deck, K. A., and W. Trautwein. 1964. Ionic currents in cardiac excitation. *Pfluegers Arch. (Eur. J. Physiol.).* 280:63–80.

Drouhard, J. P., and F. A. Roberge. 1982. The simulation of repolarization events of the cardiac Purkinje fiber action potential. *IEEE (Inst. Electr. Electron. Eng.) Trans. Biomed. Eng.* 29:481–493.

Ebihara, L., and E. A. Johnson. 1980. Fast sodium current in cardiac muscle. A quantitative description. *Biophys. J.* 32:779–790.

Ebihara, L., N. Shigeto, M. Lieberman, and E. A. Johnson. 1980. The initial inward current in spherical clusters of chick embryonic heart cells. *J. Gen. Physiol.* 75:437–456.

Eckert, R., D. L. Tillotson, and P. Brehm. 1981. Calcium mediated control of Ca and K currents. *Fed. Proc.* 40:2226–2232.

Eisenberg, B. R., and I. S. Cohen. 1983. Ultrastructure of cardiac Purkinje strand in the dog: a morphometric analysis. In press.

Eisenberg, R. S. 1983. Impedance measurement of the electrical structure of skeletal muscle. *In* Handbook of Physiology. L. D. Peachey, editor. American Physiological Society, Bethesda, MD.

Eisenberg, R. S., V. Barcilon, and R. T. Mathias. 1979. Electrical properties of spherical syncytia. *Biophys. J.* 25:151–180.

Eisenberg, R. S., and L. L. Costantin. 1971. The radial variation of potential in the transverse tubular system of skeletal muscle. *J. Gen. Physiol.* 58:700–701.

Eisenberg, R. S., and E. A. Johnson. 1970. Three dimensional electrical field problems in physiology. *Prog. Biophys. Mol. Biol.* 20:1–65.

Eisenberg, R. S., and R. T. Mathias. 1980. Structural analysis of electrical properties of cells and tissues. *CRC Crit. Rev. Bioeng.* 203–232.

Fabiato, A., and F. Fabiato. 1979. Calcium and cardiac excitation-contraction coupling. *Annu. Rev. Physiol.* 41:473–484.

Falk, G., and P. Fatt. 1964. Linear electrical properties of striated muscle fibres observed with intracellular electrodes. *Proc. R. Soc. Lond. B. Biol. Sci.* 160:69–123.

Fozzard, H. A. 1966. Membrane capacity of the cardiac Purkinje fibre. *J. Physiol. (Lond.).* 182:255–267.

Fozzard, H. A. 1977. Excitation-contraction coupling. *Annu. Rev. Physiol.* 39:201–220.

Frankenhaeuser, B., and A. L. Hodgkin. 1956. The after-effects of impulses in the giant nerve fibres of Loligo. *J. Physiol. (Lond.).* 131:341–376.

Freygang, W. H., and W. Trautwein. 1970. The structural implications of the linear electrical properties of cardiac Purkinje strands. *J. Gen. Physiol.* 55:524–547.

Gilly, Wm. F., and C. M. Armstrong. 1982a. Slowing of sodium channel opening kinetics in squid axon by extracellular zinc. *J. Gen. Physiol.* 79:935–964.

Gilly, Wm. F., and C. M. Armstrong. 1982b. Divalent cations and the activation kinetics of potassium channels in squid giant axons. *J. Gen. Physiol.* 79:965–996.

Goldman, Y., and I. M. Morad. 1977. Measurement of transmembrane potential and membrane current in cardiac muscle: a new voltage clamp method. *J. Physiol. (Lond.).* 268:613–654.

Haas, H. G., and G. Brommundt. 1980. Influence of intracellular clefts on potential and current distribution in a multifiber preparation. *Biophys. J.* 30:327–349.

Hagiwara, S., and M. Yoshii. 1979. Effects of internal potassium and sodium on the anomalous rectification of the starfish egg as examined by internal perfusion. *J. Physiol. (Lond.).* 292:251–265.

Hecht, H. H., O. F. Hutter, and D. Lywood. 1964. Voltage-current relation of short Purkinje fibres in sodium-deficient solutions. *J. Physiol. (Lond.).* 170:5P.

Heiny, J. A., and J. Vergara. 1982. Optical signals from surface and T system membranes in skeletal muscle fibers. Experiments with the potentiometric dye NK2367. *J. Gen. Physiol.* 80:203–230.

Hellam, D. C. and Studt, J. W. 1974a. Linear analysis of membrane conductance and capacitance in cardiac Purkinje fibres. *J. Physiol. (Lond.).* 243:661–694.

Hellam, D. C., and J. W. Studt. 1974b. A core-conductor model of the cardiac Purkinje fibre based on structural analysis. *J. Physiol. (Lond.).* 243:637–660.

Hille, B., and W. Schwartz. 1978. Potassium channels as multi-ion single-file pores. *J. Gen. Physiol.* 72:409–442.

Hodgkin, A. L. 1976. Chance and design in electrophysiology. *J. Physiol. (Lond.).* 263:1–21.

Hodgkin, A. L., A. F. Huxley, and B. Katz. 1952. Measurement of the current-voltage relations in the membrane of the giant axon of Loligo. *J. Physiol.* 116:424–448.

Hodgkin, A. L., and S. Nakajima. 1972. Analysis of the membrane in frog muscle. *J. Physiol. (Lond.).* 221:121–136.

Jack, J. J. B., D. Noble, and R. W. Tsien. 1975. Electric Current Flow in Excitable Cells. Clarendon Press, Oxford. 25–66.

Johnson, E. A., and M. Lieberman. 1971. Heart: excitation and contraction. *Annu. Rev. Physiol.* 33:479–532.

Joyner, R. W., M. Westerfield, J. W. Moore, and N. Stockbridge. 1978. A numerical method to model excitable cells. *Biophys. J.* 22:155–170.

Kline, R. P., and J. Kupersmith. 1982. Effects of extracellular potassium accumulation and sodium pump activation on automatic canine Purkinje fibres. *J. Physiol. (Lond.).* 324:507–533.

Lammel, E. 1981. A theoretical study on the sucrose gap technique as applied to multicellular muscle preparations. I. Saline-sucrose interdiffusion. *Biophys. J.* 36:533–553.

Leech, C. A., and P. R. Stanfield. 1981. Inward rectification in frog skeletal muscle fibres and its dependence on membrane potential and external potassium. *J. Physiol. (Lond.).* 319:295–309.

Levin, D. N., and H. A. Fozzard. 1981. A cleft model for cardiac Purkinje strands. *Biophys. J.* 33:383–408.

Levis, R. 1981. Patch and axial wire voltage clamp techniques. Ph.D. Dissertation, University California, Los Angeles, CA.

Marban, E., T. J. Rink, R. W. Tsien, and R. Y. Tsien. 1980. Free calcium in heart muscle at rest and during contraction measured with Ca^{++}-sensitive microelectrodes. *Nature (Lond.).* 286:845–850.

Marban, E., and R. W. Tsien. 1981. Is the slow inward current of heart muscle inactivated by calcium? *Biophys. J.* 33 (2, Pt. 2): 143a. (Abstr.)

Mathias, R. T. 1975. A study of the electrical properties of the transverse tubular system in skeletal muscle. Ph.D. Dissertation, University of California, Los Angeles, CA.

Mathias, R. T. 1983. The effect of tortuous extracellular pathways on resistance measurements. *Biophys. J.* 42:55–59.

Mathias, R. T., L. Ebihara, M. Lieberman, and E. A. Johnson. 1981a.

Linear electrical properties of passive and active currents in spherical heart cell clusters. *Biophys. J.* 36:221–242.

Mathias, R. T., J. L. Rae, and R. S. Eisenberg. 1981*b*. The lens as a nonuniform spherical syncytium. *Biophys. J.* 34:61–83.

Mathias, R. T., R. A. Levis, and R. S. Eisenberg. 1981*c*. An alternative interpretation of charge movement in muscle. *In* The Regulation of Muscle Contraction: Excitation-Contraction Coupling. A. D. Grinnell and M. A. B. Brazier, editor. Academic Press, Inc., New York. 39–52.

Mathias, R. T., R. S. Eisenberg, and R. Valdiosera. 1977. Electrical properties of frog skeletal muscle fibers interpreted with a mesh model of the tubular system. *Biophys. J.* 17:57–93.

Mathias, R. T., J. L. Rae, and R. S. Eisenberg. 1979. Electrical properties of structural components of the crystalline lens. *Biophys. J.* 25:181–201.

McAllister, R. E., D. Noble, and R. W. Tsien. 1975. Reconstruction of the electrical activity of cardiac Purkinje fibres. *J. Physiol. (Lond.).* 251:1–59.

Merickel, M. 1980. Design of a single electrode voltage clamp. *J. Neurosci. Methods.* 2:87–96.

Milton, R. L., R. T. Mathias, and R. S. Eisenberg. 1982. Impedance measurements at the pelvic end of frog sartorius fibers. *Biophys. J.* 37 (2, Pt. 2):356*a*. (Abstr.)

Mobley, B. A., and E. Page. 1972. The surface area of sheep cardiac Purkinje fibres. *J. Physiol. (Lond.).* 220:547–563.

Morad, M., and G. Salama. 1979. Optical probes of membrane potential in heart muscle. *J. Physiol. (Lond.).* 292:267–295.

Morad, M., and R. Weiss. 1981. Intrinsic birefringence signal preceeding the onset of contraction in heart muscle. *Science (Wash. D.C.).* 213:663–666.

Nakajima, S., and A. Gilai. 1980*a*. Action potential of isolated single muscle fibers recorded by potential-sensitive dyes. *J. Gen. Physiol.* 76:729–750.

Nakajima, S., and A. Gilai. 1980*b*. Radial propagation of muscle action potential along the tubular system examined by potential-sensitive dyes. *J. Gen. Physiol.* 76:751–762.

Noble, D. 1965. Electrical properties of cardiac muscle attributable to inward going (anomalous) rectification. *J. Cell. Comp. Physiol.* 66 (Suppl.):127–133.

Noble, D. 1975. The Initiation of the Heartbeat. Clarendon Press, Oxford University Press, Oxford, England. 1–156.

Noble, D., and R. W. Tsien. 1969. Outward membrane currents activated in the plateau range of potentials in cardiac Purkinje fibres. *J. Physiol. (Lond.).* 200:205–231.

Parsons, R. 1959. Handbook of Electrochemical Constants. Butterworths, London. 1–113.

Peskoff, A. 1979. Electric potential in cylindrical syncytia and muscle fibers. *Bull. Math. Biol.* 41:183–193.

Rae, J. L., R. T. Mathias, and R. S. Eisenberg. 1982. Physiological role of the membranes and extracellular space of within an ocular lens. *Exp. Eye Res.* 35:471–490.

Reuter, H. 1979. Properties of two inward membrane currents in the heart. *Annu. Rev. Physiol.* 41:413–424.

Reuter, H., C. F. Stevens, R. W. Tsien, and G. Yellen. 1982. Properties of single calcium channels in cardiac cell culture. *Nature (Lond.).* 297:501–504.

Schneider, M. F. 1970. Linear electrical properties of the transverse tubular and surface membrane of skeletal muscle fibers. *J. Gen. Physiol.* 56:640–671.

Schoenberg, M., G. Dominguez, and H. A. Fozzard. 1975. Effect of diameter on membrane capacity and conductance of sheep cardiac Purkinje fibers. *J. Gen. Physiol.* 65:441–458.

Schoenberg, M., and H. A. Fozzard. 1979. The influence of intercellular clefts on the electrical properties of sheep cardiac Purkinje fibers. *Biophys. J.* 25:217–234.

Sommer, J. R., and E. A. Johnson. 1968. Cardiac muscle: A comparative study of Purkinje fibers and ventricular fibers. *J. Cell. Biol.* 36:497–526.

Sommer, J. R., and E. A. Johnson. 1979. Ultrastructure of cardiac muscle. *In* Handbook of Physiology: The Cardiovascular System. R. M. Berne, N. Sperelaikis, and S. R. Geiger, editors. American Physiological Society, Bethesda, MD. 1:113–186.

Spalding, B. C., O. Senyk, J. G. Swift, and P. Horowicz. 1981. Unidirectional flux ratio for potassium ions in depolarized frog skeletal muscle. *Am. J. Physiol.* 241:C68–C75.

Sten-Knudsen, O. 1978. Passive Transport Processes. *In* Membrane Transport in Biology. Concepts and Models. D. C. Tosteson, editor. Springer-Verlag, New York, Inc., New York. 59–63.

Taylor, R. E., F. Bezanilla, and E. Rojas. 1980. Diffusion models for the squid axon Schwann cell layer. *Biophys. J.* 29:95–117.

Valdiosera, R., C. Clausen, and R. S. Eisenberg. 1974. Measurement of ‘he impedance of frog skeletal muscle fibers. *Biophys. J.* 14:295–315.

Valdiosera, R. F., and B. Mendiola. 1981. Impedance of sheep cardiac Purkinje strands. *Biophys. J.* 33(2, Pt. 2):287*a*. (Abstr.)

Wilson, W. A., and M. M. Goldner. 1975. Voltage clamping with a single microelectrode. *J. Neurobiol.* 6:411–422.